manner (11); however, unwinding *per se* may not be inducing antiviral activity. RIG-I and MDA5 contain tandem caspase recruitment and activation domain (CARD) at their amino-termini. Forced overexpression of the CARD alone is sufficient to drive antiviral signaling resulting in IFN production, showing that this domain is responsible for signaling. Indeed, the CARD of RIG-I interacts with another CARD-containing molecule, interferon-β promoter stimulator 1 (IPS-1) (also termed as MAVS, VISA, and Cardif) (12–15). Overexpression of full-length RIG-I exhibits low basal activity. Furthermore, although IFN treatment strongly induces RIG-I protein, IFN treatment alone does not activate IFN genes. Thus, an autorepression model has been proposed. It was demonstrated that a region of RIG-I acts as repression domain, which functions in *cis* as well as *trans*. LGP2 also retains repression domain; however, the corresponding region of MDA5 does not exhibit repression function. The C-terminus of RLRs consists of a domain [C-terminal domain (CTD)] and is responsible for binding with dsRNA. It has been hypothesized that binding of viral RNA with RIG-I induces conformational change in the presence of ATP to unmask CARD, but no report has experimentally demonstrated the conformational change so far.

Recognition of RNA viruses by RLRs

Based on the gene-targeting studies, it has been revealed that RLRs are essential for the production of type I IFNs and proinflammatory cytokines, such as interleukin-6 (IL-6), in response to viral infection. Double knockout cells for RIG-I and MDA5 produce no significant IFN upon viral infection, showing that these receptors are essential for sensing cytoplasmic viral RNA (16).

Cells lacking RIG-I are defective in producing type I IFNs and inflammatory cytokines in response to various RNA viruses including Newcastle disease virus (NDV) (*Paramyxoviridae*), Sendai virus (SeV) (*Paramyxoviridae*), vesicular stomatitis virus (VSV) (*Rhabdoviridae*), influenza A virus (*Orthomyxoviridae*), or Japanese encephalitis virus (JEV) (*Flaviviridae*), while MDA5-deficient cells respond normally to these viruses (16, 17). In contrast, the production of IFN in response to several picornaviruses, including encephalomyocarditis virus (EMCV), Mengo virus, and Theiler's virus, is abrogated in MDA5-deficient cells but not in cells lacking RIG-I (17, 18). Murine norovirus-1 (*Caliciviridae*) and murine hepatitis virus (*Coronaviridae*) are recognized by MDA5 (19, 20). In addition to JEV, another flavivirus, hepatitis C virus (HCV) is also recognized by RIG-I, while both RIG-I and MDA5 likely recognize Den-

gue virus and West Nile virus (*Flavivirus*), redundantly (21–23). A vaccine strain of measles virus (*Paramyxoviridae*) activates IFN through the activation of both RIG-I and MDA5, whereas the wildtype measles virus fails to induce type I IFN production (24). Reovirus, whose genome consists of segmented dsRNA, induces IFN production mainly through MDA5 with minor contribution from RIG-I (25).

Overexpression of LGP2, which lacks CARD, resulted in diminished IFN production by virus (10). However, LGP2 knockout cells exhibited attenuated IFN production upon infection of VSV or EMCV (26), suggesting that LGP2 cooperates with either RIG-I or MDA5 to sense viral RNA under physiological conditions. Influenza A virus-induced IFN production was normal in LGP2-deficient cells, suggesting that LGP2 specifically senses particular RNA patterns.

A DNA virus, Epstein–Barr virus (EBV), is reported to produce small RNAs that induce RIG-I-mediated IFN responses (27). Another DNA virus, herpes simplex virus (HSV), is also reported to activate both RIG-I- and MDA5-dependent IFN responses via dsRNA produced during its replication (28).

RNA ligands of RLRs

Polyriboinosinic:polyribocytidylic acid

Polyriboinosinic:polyribocytidylic acid (polyI:C), a synthetic dsRNA, which was selected as a potent non-viral IFN inducer, acts as a ligand for TLR3 and RLRs (4, 25). Although the mechanism underlying is not known, poly I:C exhibits highest activity among the possible combinations of RNA homopolymer duplexes. Poly I:C is generated by annealing poly I and poly C, which are synthesized by polynucleotide phosphorylase. This enzyme catalyzes the polymerization of nucleotide diphosphate, thus poly I:C harbors a 5′-diphosphate (29).

Two groups demonstrated that MDA5 is essential for poly I:C-mediated IFN production by gene targeting (16, 18). The specificity originates from the length of dsRNA rather than base composition (25). Commercial poly I:C runs as dsRNA of 4–8 kbp in gel electrophoresis. Partial digestion of the poly I:C with a dsRNA specific endonuclease, RNaseIII, led to the generation of trimmed poly I:C of about 300 bp. This short poly I:C activates RIG-I. Interestingly, short poly I:C fails to activate MDA5, and long poly I:C is incapable of activating RIG-I, although both of these bind to long and short poly I:C. Therefore, both RIG-I and MDA5 are necessary to sense various length of dsRNA. The precise mechanism of size discrimination by RIG-I and MDA5 is not known.

5′ tri-phosphate RNAs

RNA transcribed from DNA template by T7 RNA polymerase is a strong inducer of type I IFN (30). Further studies revealed that 5′-triphosphate containing RNA, such as genomes of most RNA viruses, and in vitro transcripts are selectively recognized by RIG-I (31, 32). Since the 5′-triphosphate moieties of most host transcripts are removed by adding 7-methyl-guanosine cap (in the case of mRNA) or by processing (tRNA and rRNA), these self-RNAs are refractory to detection by RIG-I. However more recently, it was revealed that 5′-triphosphate per se is not sufficient for RIG-I activation. This is consistent with observations that dsRNA without 5′-triphosphate can be recognized by RIG-I particularly for long dsRNA. Therefore, dsRNA structure is prerequisite for RIG-I activation and 5′-triphosphate facilitates the recognition of short dsRNA. In addition, removal of 5′-triphosphate is a viral strategy to avoid recognition by RIG-I. A viral peptide, VPg, is covalently attached to the 5′ end of Picornaviridae RNA, thus lacking 5′-triphosphate (33). Hantaan virus (HTNV), Crimean-Congo hemorrhagic fever virus (CCHFV) (Bunyaviridae), and Borna disease virus (BDV) (Bornaviridae) do not trigger RIG-I-mediated IFN responses, because the 5′-triphosphate structure of these viral genomic RNA is removed by processing (34).

Transfection of AT-rich dsDNA (typically a synthetic poly-dAdT:polydAdT) results in the type I IFN induction(35). It was revealed that polydAdT:polydAdT is transcribed by host DNA-dependent RNA polymerase III and that the resultant 5′-triphosphate dsRNA is detected by RIG-I (36, 37). The polymerase III-mediated mechanism may explain IFN induction by some DNA viruses or intracellular bacteria.

Nallagatla et al. (38) suggested that the 5′ tri-phosphate signature is sensed by protein kinase R (PKR) in addition to dsRNA. Further studies are required to elucidate the mechanism by which the 5′ tri-phosphate signature activates both RIG-I and PKR and to understand its biological significance.

Viral RNA ligand for RLR

Garcin's group (39) nicely showed this dsRNA-dependent activation of RIG-I, using a SeV infection. They generated SeV expressing GFP mRNA or antisense GFP mRNA and performed co-infection of two types of SeV. They found that the resulting capped dsRNA of GFP sequences induced an IFN response that was dependent on RIG-I. In addition to engineered SeV, natural VSV, a ssRNA virus recognized by RIG-I, was shown to produce dsRNA in infected cells (25). Induction of IFNs by

RNAs from VSV-infected cells was impaired by disrupting dsRNA, suggesting the presence of dsRNA in VSV-infected cells is important for RIG-I mediated IFN responses. The fragments produced by VSV were about 2–2.5 kbp much shorter than the length of the 11 kb VSV genomic RNA, suggesting that these dsRNA were not derived from replication intermediates of VSV. Rather, the dsRNA maybe be derived from defective interfering (DI) particles, whose snap-back dsRNAs are reported to be about 2.2 kbp, generated in VSV-infected cells, although the viral dsRNA signiture recognized by RIG-I remains to be further characterized. Recently, panhandle structure of the influenza virus genome is also reported as RIG-I ligand (40). It is of interest to clarify which ligand is the major source of RIG-I-dependent IFN production in individual viral infection.

IFN production induced by long segments purified from the reovirus genome (about 3.9 kbp) is impaired in MDA5-deficient cells (25). Further, the very large RNA species (stuck at the top of the gel during electrophoresis) generated by EMCV or vaccinia virus infection is a specific ligand for MDA5 (41). Although the precise structure of the RNA (termed RNA web), is not known, a highly ordered structure is critical for this activity, as heat treatment inactivated the complex.

RNaseL-cleaved RNA

RNaseL is an endonuclease thought to cleave viral RNA. Silverman's group (42) showed that RNaseL-deficient cells showed attenuated induction of IFN in response to poly I:C or Sendai virus. In addition, in the infection with EMCV and Sendai virus, RNaseL-deficient mice showed impaired IFN production in sera. The RNaseL cleavage products activate RIG-I and MDA5, leading to production of type I IFNs. This mechanism potentially generates RLR ligands from self-RNA as well as viral RNA.

Poly-U/UC rich RNA

Infection with HCV is known to be regulated by hepatic immune defense triggered by RIG-I. Mapping of the HCV genome for RIG-I activation revealed that 5′-triphosphate signature was necessary but not sufficient for the activation of RIG-I and that a polyuridine motif (poly-U/UC-rich region) at the 3′-non-translated region is critical for efficient activation of RIG-I (43). They extended their finding and found that 5′-triphosphate genomic poly-U/A-rich RNA motifs within the rabies virus leader sequence, Ebola virus 3′ region, and measles virus leader sequence were also important for RIG-I

activation (43). However, GC-rich RNA motifs failed to induce the signaling (43). Thus, A/U composition and poly-U motifs are possible determinants of viral RNA recognition by antiviral innate immunity. Representative RNA patterns and recognizing RLRs are summarized in Fig. 1.

Structure of RLRs

Two groups independently identified the RNA recognition domain that is located to the C-terminus to the helicase domain CTD. Takahasi et al. (11) showed that RIG-I CTD specifically binds dsRNA and 5′-triphosphate RNA and solved its solution structure. Furthermore, these studies revealed that large positive charged surface that locates the center of the structure is the RNA binding site by NMR titration (11). Cui et al. also identified the domain and solved the crystal structure (44). The structures of MDA5 and LGP2 CTDs were also solved and their structural features are very similar to RIG-I CTD (45). Recent studies have solved the crystal structures of RIG-I CTD bound to both blunt ended double-strand RNA and dsRNA with 5′-triphosphate (46–48). Both CTD structures showed that the same basic surface revealed in previous studies was essential for the RNA recognition. However, two different ended RNAs bound RIG-I CTD in different orientations (46–48). The complex structure of LGP2 bound to the blunt end of dsRNA was also solved by x-ray crystallography, but the orientation of the RNA in the complex was also different from the RNAs bound to the RIG-I CTD (49). The biological

significance of these co-crystals requires further investigation because the biological activity of the RNA used for crystal is not well investigated, particularly the presence or absence of 5′-triphosphate. These observations imply that RIG-I specifically recognizes the end structure of viral RNA, especially blunt end dsRNA or 5′-triphosphate structure. However, it has been controversial if end structure affects recognition by RIG-I (11, 45, 46). In addition, AFM analysis suggests that RIG-I aggregates around the short poly I:C, excluding the possibility of end-specific binding (25). For certain, better understanding of the activation of the RIG-I/RNA complex awaits further structural elucidation of inactive (free RIG-I in closed structure) and activated (RIG-I/RNA complex in the presence of ATP) complexes.

RLR signaling and its regulation

Upon binding to viral RNA in the presence of ATP, RIG-I changes its conformation to expose the CARD. The activated RIG-I forms oligomer, which allows the CARDs of RIG-I to interact with a CARD-containing adapter, IPS-1, which is localized on the outer membrane of the mitochondrion. MDA5 also transduces signaling via IPS-1. IPS-1 subsequently activates two IκB kinase (IKK)-related kinases, IKK-i, and TANK-binding kinase 1 (TBK1) via tumor necrosis factor (TNF) receptor-associated factor 3 (TRAF3) (50–52). These kinases phosphorylate IRF3 and IRF7, resulting in their
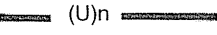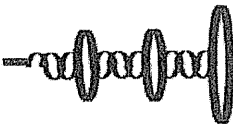

RNA	Structure	RLR	Ref
A Long polyI:C	5'PP ... PP5'	MDA5	25 16,18
B Short polyI:C (short dsRNA without 5' triphosphates)		RIG-I	25
C 5' triphosphate RNAs (generated by T7 polymerase)	5'PPP	RIG-I	31,32
D poly U/UC rich RNA (HCV)	5'PPP (U)n	RIG-I	43
E Panhandle region of Influenza virus genome		RIG-I	40
F RNaseL-cleaved self RNAs	3'p ... p3'	RIG-I MDA5	42
G RNA web (higher order structure)		MDA5	41

Fig. 1. **RNA patterns and their recognition by RLRs.** Summary of synthetic and viral RNA patterns and the RLRs recognizing them.

181

translocation from the cytoplasm into the nucleus, which activates transcription of genes encoding type I IFNs and IFN-inducible genes (53, 54). In addition, IPS-1 activates NF-κB via a FADD and caspase-8/10 pathway to regulate the expression of proinflammatory cytokine genes (55).

Many molecules have been reported to modulate the RLR-mediated signaling pathway (described above) through direct interaction with RLRs or with signaling molecules. For instance, Src homology 2 (SH2) domain-containing phosphatase-1 (SHP-1) is reported to activate RIG-I-mediated signaling by binding directly to RIG-I (56). Dihydroacetone kinase (DAK) was identified as a MDA5-interacting protein and was shown to negatively regulate MDA5 (57). NLRX1 (also known as NOD9) is localized to the mitochondrial outer membranes and is suggested to function as a negative regulator of IPS-1 via a direct interaction (58). Suppressor of IKKε (SIKE) forms a complex with TBK1/IKKε and inhibits the interaction of RIG-I or IRFs with TBK1/IKKε in the basal condition, while viral infection leads to dissociation of SIKE from TBK/IKKε (59). Molecules involved in the autophagic machinery, Atg5-atg12, are reported to inhibit the interaction

between RIG-I and IPS-1 by association with the CARD of RIG-I and with IPS-1 (60). Recent studies from two independent groups (61, 62) identified the same signal-modulator molecule, designated as stimulator of IFN genes (STING), also called mediator of IRF-3 activation (MITA). STING is reported to localize to the endoplasmic reticulum (ER) membrane, and STING interacts with RIG-I (but not MDA5), and SSR2/TRPβ complex, required for protein translocation across the ER membrane. The other group reported that STING is expressed on the outer membrane of mitochondrion, where it interacts directly with IPS-1 and IRF-3 and positively regulates the virus-dependent recruitment of TBK1 to the IPS-1 complex on mitochondrion.

Ubiquitination of RLRs is reported to control their signals both positively and negatively. The CARDs of RIG-I undergo Lys63-linked ubiquitination by tripartite motif 25 (TRIM 25), and this ubiquitination is necessary for efficient activation of RIG-I mediated signaling (63). Interestingly, MDA5 does not undergo ubiquitination by TRIM25, suggesting that CARDs of RIG-I and MDA5 are differentially regulated. A tumor suppressor, CYLD (cylindomatosis), is reported to negatively regulate
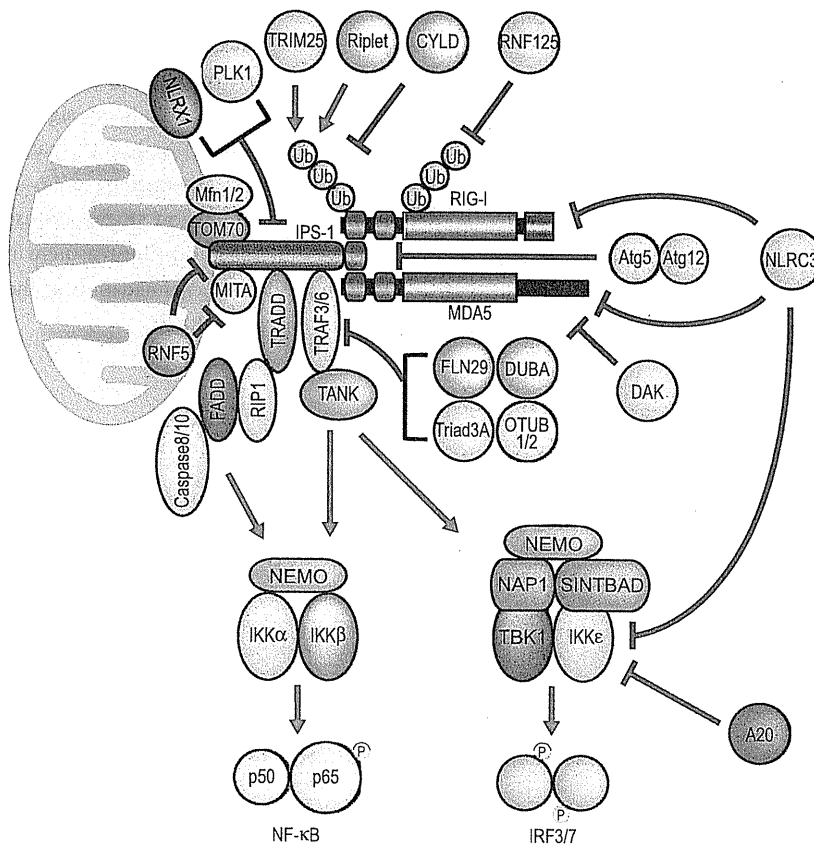

Fig. 2. **RLR-mediated signaling and adapter molecules.** Positive and negative regulation is indicated by red and blue lines, respectively.

95

the RIG-I-mediated signaling by deubiquitinating the TRIM25-mediated ubiquitination of RIG-I (64). Another E3 ubiquitin ligase RNF135/Riplet is shown to promote Lys63-linked ubiquitination of the C-terminal region of RIG-I, which results in activation of IFN promoter (65). RIG-I also undergoes Lys48-linked polyubiquitination by the E3 ubiquitin ligase RNF125, leading to its proteasomal degradation, which inhibits aberrant activation of RIG-I mediated signaling. Further, RNF125 conjugates ubiquitin to MDA5 as well as IPS-1, which results in suppressing the functions of these proteins (66). It was also recently shown that REUL is an E3 ubiquitin ligase of RIG-I and specifically stimulates RIG-I-mediated IFN signaling (67). The Lys 154, 164, and 172 residues of the RIG-I CARD domain are critical for efficient REUL-mediated ubiquitination, as well as the ability of RIG-I to induce activation of the IFN-β promoter. ISGylation also modulates RLR-signaling. RIG-I is ISGylated by the ubiquitin-like protein, ISG15, which regulates the activity of RNF125 together with UbcH8, an E2 ubiquitin-conjugating enzyme (68). UbcH8 suppresses ubiquitination of RIG-I by RNF125, and the suppression by UbcH8 is relieved by ISG15.

Artificial aggregation of IPS-1 in the cytoplasm is sufficient for activation of antiviral signaling (69), suggesting that the activity of IPS-1 is regulated by its oligomerization induced by physical interaction of CARD of RIG-I or MDA5. Interestingly, IPS-1 aggregation is observed in cells stably expressing Flag-tagged IPS-1 upon infection by various viruses or 5'-triphosphate RNA. Normally IPS-1 is localized on the outer membrane of the mitochondrion, which may restrict its movement. The IPS-1 aggregation requires mitofusin 1, a mitochondrial regulator for its fusion (70). Mitofusin 1 is also reported to be critical for mitochondrial elongation induced by certain strains of Sendai virus. These results suggest that the activity of IPS-1 requires dynamic fission and fusion of mitochondrion to facilitate efficient signaling by its oligomerization. However, there are contradictory reports on the function of mitochondrion and mitofusins (71). The adaptor molecules involved in RLR-mediated signaling are summarized in Fig. 2.

In addition to host regulatory factors mentioned above, viruses acquire means to evade antiviral immunity of the host. Modification of viral RNA and assembly of nucleocapsid are major strategies to escape from detection by RLRs. Viral nonstructural (NS) proteins often participate in the counteraction of antiviral cascades. A large number of viral inhibitory proteins have been identified that block RLR signaling at various levels (reviewed in 72, 73).

Conclusions and perspectives

Cumulative studies based on RLR knockout mice/cells and various viruses revealed the mechanism by which RLRs sense viral invasion as well as viral strategies to evade antiviral responses mediated by RLRs. As described in this review, it is clear that RIG-I and MDA5 are essential sensors for RNA viruses and that these helicases discriminate self and non-self RNAs by precise recognition of virus-specific RNA signatures. However, elucidation of many signaling regulators has made the picture more complicated than previously appreciated. Certainly, many interesting topics remain to be clarified, including identification of the precise RNA ligands of RLRs during viral infection, the reason why IPS-1 localizes to the mitochondrion, and elucidation of the molecular structure of inactive and active RIG-I.

References

1. Takeuchi O, Akira S. Pattern recognition receptors and inflammation. Cell 2010;140:805–820.
2. Fujita T. A nonself RNA pattern: tri-p to panhandle. Immunity 2009;31:4–5.
3. Beutler B, et al. Genetic analysis of resistance to viral infection. Nat Rev Immunol 2007;7:753–766.
4. Alexopoulou L, Holt AC, Medzhitov R, Flavell RA. Recognition of double-stranded RNA and activation of NF-kappaB by Toll-like receptor 3. Nature 2001;413:732–738.
5. Heil F, et al. Species-specific recognition of single-stranded RNA via toll-like receptor 7 and 8. Science 2004;303:1526–1529.
6. Diebold SS, Kaisho T, Hemmi H, Akira S, Reis e Sousa C. Innate antiviral responses by means of TLR7-mediated recognition of single-stranded RNA. Science 2004;303:1529–1531.
7. Hemmi H, et al. Small anti-viral compounds activate immune cells via the TLR7 MyD88-dependent signaling pathway. Nat Immunol 2002;3:196–200.
8. Hemmi H, et al. A Toll-like receptor recognizes bacterial DNA. Nature 2000;408:740–745.
9. Yoneyama M, et al. The RNA helicase RIG-I has an essential function in double-stranded RNA-induced innate antiviral responses. Nat Immunol 2004;5:730–737.
10. Yoneyama M, et al. Shared and unique functions of the DExD/H-box helicases RIG-I, MDA5, and LGP2 in antiviral innate immunity. J Immunol 2005;175:2851–2858.
11. Takahasi K, et al. Nonself RNA-sensing mechanism of RIG-I helicase and activation of antiviral immune responses. Mol Cell 2008;29:428–440.
12. Kawai T, et al. IPS-1, an adaptor triggering RIG-I- and Mda5-mediated type I interferon induction. Nat Immunol 2005;6:981–988.
13. Xu LG, Wang YY, Han KJ, Li LY, Zhai Z, Shu HB. VISA is an adapter protein required for virus-triggered IFN-beta signaling. Mol Cell 2005;19:727–740.

14. Seth RB, Sun L, Ea CK, Chen ZJ. Identification and characterization of MAVS, a mitochondrial antiviral signaling protein that activates NF-kappaB and IRF 3. Cell 2005;**122**:669–682.

15. Meylan E, et al. Cardif is an adaptor protein in the RIG-I antiviral pathway and is targeted by hepatitis C virus. Nature 2005;**437**:1167–1172.

16. Kato H, et al. Differential roles of MDA5 and RIG-I helicases in the recognition of RNA viruses. Nature 2006;**441**:101–105.

17. Kato H, et al. Cell type-specific involvement of RIG-I in antiviral response. Immunity 2005;**23**:19–28.

18. Gitlin L, et al. Essential role of mda-5 in type I IFN responses to polyriboinosinic: polyribocytidylic acid and encephalomyocarditis picornavirus. Proc Natl Acad USA 2006;**103**:8459–8464.

19. McCartney SA, Thackray LB, Gitlin L, Gilfillan S, Virgin HW, Colonna M. MDA-5 recognition of a murine norovirus. PLoS Pathog 2008;**4**:e1000108.

20. Roth-Cross JK, Bender SJ, Weiss SR. Murine coronavirus mouse hepatitis virus is recognized by MDA5 and induces type I interferon in brain macrophages/microglia. J Virol 2008;**82**:9829–9838.

21. Foy E, et al. Control of antiviral defenses through hepatitis C virus disruption of retinoic acid-inducible gene-I signaling. Proc Natl Acad Sci USA 2005;**102**:2986–2991.

22. Loo YM, et al. Distinct RIG-I and MDA5 signaling by RNA viruses in innate immunity. J Virol 2008;**82**:335–345.

23. Fredericksen BL, Gale M Jr. West Nile virus evades activation of interferon regulatory factor 3 through RIG-I-dependent and -independent pathways without antagonizing host defense signaling. J Virol 2006;**80**:2913–2923.

24. Shingai M, et al. Differential type I IFN-inducing abilities of wild-type versus vaccine strains of measles virus. J Immunol 2007;**179**:6123–6133.

25. Kato H, et al. Length-dependent recognition of double-stranded ribonucleic acids by retinoic acid-inducible gene-I and melanoma differentiation-associated gene 5. J Exp Med 2008;**205**:1601–1610.

26. Satoh T, et al. LGP2 is a positive regulator of RIG-I- and MDA5-mediated antiviral responses. Proc Natl Acad Sci USA 2010;**107**:1512–1517.

27. Samanta M, Iwakiri D, Kanda T, Imaizumi T, Takada K. EB virus-encoded RNAs are recognized by RIG-I and activate signaling to induce type I IFN. EMBO J 2006;**25**:4207–4214.

28. Rasmussen SB, et al. Herpes simplex virus infection is sensed by both Toll-like receptors and retinoic acid-inducible gene-like receptors, which synergize to induce type I interferon production. J Gen Virol 2009;**90**:74–78.

29. Grunberg-Manago M, Oritz PJ, Ochoa S. Enzymatic synthesis of nucleic acidlike polynucleotides. Science 1955;**122**:907–910.

30. Kim DH, Longo M, Han Y, Lundberg P, Cantin E, Rossi JJ. Interferon induction by siRNAs and ssRNAs synthesized by phage polymerase. Nat Biotechnol 2004;**22**:321–325.

31. Hornung V, et al. 5'-Triphosphate RNA is the ligand for RIG-I. Science 2006;**314**:994–997.

32. Pichlmair A, et al. RIG-I-mediated antiviral responses to single-stranded RNA bearing 5'-phosphates. Science 2006;**314**:997–1001.

33. Pallansch MA, Kew OM, Palmenberg AC, Golini F, Wimmer E, Rueckert RR. Picornaviral VPg sequences are contained in the replicase precursor. J Virol 1980;**35**:414–419.

34. Habjan M, et al. Processing of genome 5' termini as a strategy of negative-strand RNA viruses to avoid RIG-I-dependent interferon induction. PLoS ONE 2008;**3**:e2032.

35. Ishii KJ, et al. A Toll-like receptor-independent antiviral response induced by double-stranded B-form DNA. Nat Immunol 2006;**7**:40–48.

36. Ablasser A, Bauernfeind F, Hartmann G, Latz E, Fitzgerald KA, Hornung V. RIG-I-dependent sensing of poly(dA:dT) through the induction of an RNA polymerase III-transcribed RNA intermediate. Nat Immunol 2009;**10**:1065–1072.

37. Chiu YH, MacMillan JB, Chen ZJ. RNA polymerase III detects cytosolic DNA and induces type i interferons through the RIG-I pathway. Cell 2009;**138**:576–591.

38. Nallagatla SR, Hwang J, Toroney R, Zheng X, Cameron CE, Bevilacqua PC. 5'-triphosphate-dependent activation of PKR by RNAs with short stem-loops. Science 2007;**318**:1455–1458.

39. Hausmann S, Marq JB, Tapparel C, Kolakofsky D, Garcin D. RIG-I and dsRNA-induced IFNbeta activation. PLoS ONE 2008;**3**:e3965.

40. Rehwinkel J, et al. RIG-I detects viral genomic RNA during negative-strand RNA virus infection. Cell 2010;**140**:397–408.

41. Pichlmair A, et al. Activation of MDA5 requires higher-order RNA structures generated during virus infection. J Virol 2009;**83**:10761–10769.

42. Malathi K, Dong B, Gale M Jr, Silverman RH. Small self-RNA generated by RNase L amplifies antiviral innate immunity. Nature 2007;**448**:816–819.

43. Saito T, Owen DM, Jiang F, Marcotrigiano J, Gale M Jr. Innate immunity induced by composition-dependent RIG-I recognition of hepatitis C virus RNA. Nature 2008;**454**:523–527.

44. Cui S, et al. The C-terminal regulatory domain is the RNA 5'-triphosphate sensor of RIG-I. Mol Cell 2008;**29**:169–179.

45. Takahasi K, et al. Solution structures of cytosolic RNA sensor MDA5 and LGP2 C-terminal domains: identification of the RNA recognition loop in RIG-I-like receptors. J Biol Chem 2009;**284**:17465–17474.

46. Lu C, et al. The structural basis of 5' triphosphate double-stranded RNA recognition by RIG-I C-terminal domain. Structure 2010;**18**:1032–1043.

47. Wang Y, et al. Structural and functional insights into 5'-ppp RNA pattern recognition by the innate immune receptor RIG-I. Nat Struct Mol Biol 2010;**17**:781–787.

48. Lu C, Ranjith-Kumar CT, Hao L, Kao CC, Li P. Crystal structure of RIG-I C-terminal domain bound to blunt-ended double-strand RNA without 5' triphosphate. Nucleic Acids Res 2011;**39**:1565–1575.

49. Li X, et al. The RIG-I-like receptor LGP2 recognizes the termini of double-stranded RNA. J Biol Chem 2009;**284**:13881–13891.

50. Fitzgerald KA, et al. IKKepsilon and TBK1 are essential components of the IRF3 signaling pathway. Nat Immunol 2003;**4**:491–496.

51. Hemmi H, et al. The roles of two IkappaB kinase-related kinases in lipopolysaccharide and double stranded RNA signaling and viral infection. J Exp Med 2004;**199**:1641–50.

52. Häcker H, et al. Specificity in Toll-like receptor signalling through distinct effector functions of TRAF3 and TRAF6. Nature 2006;**439**:204–207.

53. Sato M, et al. Distinct and essential roles of transcription factors IRF-3 and IRF-7 in response to viruses for IFN-alpha/beta gene induction. Immunity 2000;**13**:539–548.

54. Honda K, et al. IRF-7 is the master regulator of type-I interferon-dependent immune responses. Nature 2005;**434**:772–777.

55. Takahashi K, Kawai T, Kumar H, Sato S, Yonehara S, Akira S. Roles of caspase-8 and caspase-10 in innate immune responses to double-stranded RNA. J Immunol 2006;**176**:4520–4524.

56. An H, et al. Phosphatase SHP-1 promotes TLR- and RIG-I-activated production of type I interferon by inhibiting the kinase IRAK1. Nat Immunol 2008;**9**:542–550.

57. Diao F, et al. Negative regulation of MDA5-but not RIG-I-mediated innate antiviral signaling by the dihydroxyacetone kinase. Proc Natl Acad Sci USA 2007;**104**:11706–11.

58. Moore CB, et al. NLRX1 is a regulator of mitochondrial antiviral immunity. Nature 2008;**451**:573–577.

59. Huang J, Liu T, Xu LG, Chen D, Zhai Z, Shu HB. SIKE is an IKKε/TBK1-associated suppressor of TLR3- and virus-triggered IRF-3

activation pathways. EMBO J 2005;**24**:4018–4028.

60. Jounai N, et al. The Atg5-Atg12 conjugate associates with innate antiviral immune responses. Proc Natl Acad Sci USA 2007;**104**:14050–14055.

61. Ishikawa H, Barber GN. STING is an endoplasmic reticulum adaptor that facilitates innate immune signalling. Nature 2008;**455**:674–678.

62. Zhong B, et al. The adaptor protein MITA links virus-sensing receptors to IRF3 transcription factor activation. Immunity 2008;**29**:538–550.

63. Gack MU, et al. TRIM25 RING-finger E3 ubiquitin ligase is essential for RIG-I-mediated antiviral activity. Nature 2007;**446**:916–920.

64. Friedman CS, et al. The tumour suppressor CYLD is a negative regulator of RIG-I-mediated antiviral response. EMBO Rep 2008;**9**:930–936.

65. Oshiumi H, Matsumoto M, Hatakeyama S, Seya T. Riplet/RNF135, a RING finger protein, ubiquitinates RIG-I to promote interferon-β induction during the early phase of viral infection. J Biol Chem 2009;**284**:807–817.

66. Arimoto KI, Takahashi H, Hishiki T, Konishi H, Fujita T, Shimotohno K. Negative regulation of the RIG-I signaling by the ubiquitin ligase RNF125. Proc Natl Acad Sci USA 2007;**104**:7500–7505.

67. Gao D, et al. REUL is a novel E3 ubiquitin ligase and stimulator of retinoic-acid-inducible gene-I. PLoS ONE 2009;**4**:e5760.

68. Arimoto KI, Konishi H, Shimotohno K. UbcH8 regulates ubiquitin and ISG15 conjugation to RIG-I. Mol Immunol 2008;**45**:1078–1084.

69. Tang ED, Wang CY. MAVS self-association mediates antiviral innate immune signaling. J Virol 2009;**83**:3420–8.

70. Onoguchi K, et al. Virus-infection or 5′ppp-RNA activates antiviral signal through redistribution of IPS-1 mediated by MFN1. PLoS Pathog 2010;**6**:e1001012.

71. Yasukawa K, et al. Mitofusin 2 inhibits mitochondrial antiviral signaling. Sci Signal 2009;**2**:ra47.

72. Bowie AG, Unterholzner L. Viral evasion and subversion of pattern-recognition receptor signalling. Nat Rev Immunol 2008;**8**:911–922.

73. Komuro A, Bamming D, Horvath CM. Negative regulation of cytoplasmic RNA-mediated antiviral signaling. Cytokine 2008;**43**:350–358.

Hepatitis C Virus Hijacks P-Body and Stress Granule Components around Lipid Droplets[▽]

Yasuo Ariumi,[1,2]* Misao Kuroki,[1] Yukihiro Kushima,[3] Kanae Osugi,[4] Makoto Hijikata,[3] Masatoshi Maki,[4] Masanori Ikeda,[1] and Nobuyuki Kato[1]

Department of Tumor Virology, Okayama University Graduate School of Medicine, Dentistry, and Pharmaceutical Sciences, Okayama 700-8558, Japan[1]; Center for AIDS Research, Kumamoto University, Kumamoto 860-0811, Japan[2]; Department of Viral Oncology, Institute for Virus Research, Kyoto University, Kyoto 606-8507, Japan[3]; and Department of Applied Molecular Biosciences, Graduate School of Bioagricultural Sciences, Nagoya University, Nagoya 464-8601, Japan[4]

The microRNA miR-122 and DDX6/Rck/p54, a microRNA effector, have been implicated in hepatitis C virus (HCV) replication. In this study, we demonstrated for the first time that HCV-JFH1 infection disrupted processing (P)-body formation of the microRNA effectors DDX6, Lsm1, Xrn1, PATL1, and Ago2, but not the decapping enzyme DCP2, and dynamically redistributed these microRNA effectors to the HCV production factory around lipid droplets in HuH-7-derived RSc cells. Notably, HCV-JFH1 infection also redistributed the stress granule components GTPase-activating protein (SH3 domain)-binding protein 1 (G3BP1), ataxin-2 (ATX2), and poly(A)-binding protein 1 (PABP1) to the HCV production factory. In this regard, we found that the P-body formation of DDX6 began to be disrupted at 36 h postinfection. Consistently, G3BP1 transiently formed stress granules at 36 h postinfection. We then observed the ringlike formation of DDX6 or G3BP1 and colocalization with HCV core after 48 h postinfection, suggesting that the disruption of P-body formation and the hijacking of P-body and stress granule components occur at a late step of HCV infection. Furthermore, HCV infection could suppress stress granule formation in response to heat shock or treatment with arsenite. Importantly, we demonstrate that the accumulation of HCV RNA was significantly suppressed in DDX6, Lsm1, ATX2, and PABP1 knockdown cells after the inoculation of HCV-JFH1, suggesting that the P-body and the stress granule components are required for the HCV life cycle. Altogether, HCV seems to hijack the P-body and the stress granule components for HCV replication.

Hepatitis C virus (HCV) is the causative agent of chronic hepatitis, which progresses to liver cirrhosis and hepatocellular carcinoma. HCV is an enveloped virus with a positive single-stranded 9.6-kb RNA genome, which encodes a large polyprotein precursor of approximately 3,000 amino acid (aa) residues. This polyprotein is cleaved by a combination of the host and viral proteases into at least 10 proteins in the following order: core, envelope 1 (E1), E2, p7, nonstructural 2 (NS2), NS3, NS4A, NS4B, NS5A, and NS5B (12, 13, 21). The HCV core protein, a nucleocapsid, is targeted to lipid droplets (LDs), and the dimerization of the core protein by a disulfide bond is essential for the production of infectious virus (24). Recently, LDs have been found to be involved in an important cytoplasmic organelle for HCV production (26). Budding is an essential step in the life cycle of enveloped viruses. The endosomal sorting complex required for transport (ESCRT) system has been involved in such enveloped virus budding machineries, including that of HCV (5).

DEAD-box RNA helicases with ATP-dependent RNA-unwinding activities have been implicated in various RNA metabolic processes, including transcription, translation, RNA splicing, RNA transport, and RNA degradation (32). Previously, DDX3 was identified as an HCV core-interacting pro-

tein by yeast two-hybrid screening (25, 29, 43). Indeed, DDX3 is required for HCV RNA replication (3, 31). DDX6 (Rck/p54) is also required for HCV replication (16, 33). DDX6 interacts with an initiation factor, eukaryotic initiation factor 4E (eIF-4E), to repress the translational activity of mRNP (38). Furthermore, DDX6 regulates the activity of the decapping enzymes DCP1 and DCP2 and interacts directly with Argonaute-1 (Ago1) and Ago2 in the microRNA (miRNA)-induced silencing complex (miRISC) and is involved in RNA silencing. DDX6 localizes predominantly in the discrete cytoplasmic foci termed the processing (P) body. Thus, the P body seems to be an aggregate of translationally repressed mRNPs associated with the translation repression and mRNA decay machinery.

In addition to the P body, eukaryotic cells contain another type of RNA granule termed the stress granule (SG) (1, 6, 22, 30). SGs are aggregates of untranslating mRNAs in conjunction with a subset of translation initiation factors (eIF4E, eIF3, eIF4A, eIFG, and poly(A)-binding protein [PABP]), the 40S ribosomal subunits, and several RNA-binding proteins, including PABP, T cell intracellular antigen 1 (TIA-1), TIA-1-related protein (TIAR), and GTPase-activating protein (SH3 domain)-binding protein 1 (G3BP1). SGs regulate mRNA translation and decay as well as proteins involved in various aspects of mRNA metabolisms. SGs are cytoplasmic phase-dense structures that occur in eukaryotic cells exposed to various environmental stress, including heat, arsenite, viral infection, oxidative conditions, UV irradiation, and hypoxia. Impor-

---

* Corresponding author. Mailing address: Center for AIDS Research, Kumamoto University, 2-2-1 Honjo, Kumamoto 860-0811, Japan. Phone and fax: 81 96 373 6834. E-mail: ariumi@kumamoto-u.ac.jp.

tantly, several viruses target SGs and stress granule components for viral replication (10, 11, 34, 39). Recent studies suggest that SGs and the P body physically interact and that mRNAs may move between the two compartments (1, 6, 22, 28, 30).

miRNAs are a class of small noncoding RNA molecules ~21 to 22 nucleotides (nt) in length. miRNAs usually interact with 3'-untranslated regions (UTRs) of target mRNAs, leading to the downregulation of mRNA expression. Notably, the liver-specific and abundant miR-122 interacts with the 5'-UTR of the HCV RNA genome and facilitates HCV replication (15, 17, 19, 20, 31). Ago2 is at least required for the efficient miR-122 regulation of HCV RNA accumulation and translation (40). However, the molecular mechanism(s) for how DDX6 and miR-122 as well as DDX3 positively regulate HCV replication is not fully understood. Therefore, we investigated the potential role of P-body and stress granule components in HCV replication.

MATERIALS AND METHODS

Cell culture. 293FT cells were cultured in Dulbecco's modified Eagle's medium (DMEM; Invitrogen, Carlsbad, CA) supplemented with 10% fetal bovine serum (FBS). HuH-7-derived RSc cured cells, in which cell culture-generated HCV-JFH1 (JFH1 strain of genotype 2a) (37) could infect and effectively replicate, were cultured in DMEM with 10% FBS as described previously (3–5, 23).

Plasmid construction. To construct pcDNA3-FLAG-DDX6, a DNA fragment encoding DDX6 was amplified from total RNAs derived from RSc cells by reverse transcription (RT)-PCR using KOD-Plus DNA polymerase (Toyobo) and the following pairs of primers: 5'-CGGGATCCAAGATGAGCACGGCC AGAACAGAGAACCCTGTT-3' (forward) and 5'-CCGCTCGAGTTAAGGT TTCTCATCTTCTACAGGCTCGCT-3' (reverse). The obtained DNA fragments were subcloned into either BamHI-XhoI site of the pcDNA3-FLAG vector (2), and the nucleotide sequences were determined by BigDye termination cycle sequencing using an ABI Prism 310 genetic analyzer (Applied Biosystems, Foster City, CA).

RNA interference. The following small interfering RNAs (siRNAs) were used: human ATXN2/ATX2/ataxin-2 (siGENOME SMRT pool M-011772-01-005), human PABP1/PABPC1 (siGENOME SMRT pool M-019598-01-005), human Lsm1 (siGENOME SMRT pool M-005124-01-005), human Xrn1 (siGENOME SMRT pool M-013754-01-005), human G3BP1 (ON-TARGETplus SMRT pool L-012099-00-005), human PATL1 (siGENOME SMRT pool M-015591-00-005), and siGENOME nontargeting siRNA pool 1 (D-001206-13-05) (Dharmacon, Thermo Fisher Scientific, Waltham, MA), as a control. siRNAs (25 nM final concentration) were transiently transfected into RSc cells (3–5, 23) using Oligofectamine (Invitrogen) according to the manufacturer's instructions. Oligonucleotides with the following sense and antisense sequences were used for the cloning of short hairpin RNA (shRNA)-encoding sequences targeted to DDX6 (DDX6i) as well as the control nontargeting shRNA (shCon) in a lentiviral vector: 5'-GATCC CCGGAGGAACTAACTCTGAAGTTCAAGAGACTTCAGAGTTAGTTCCT CCTTTTTGGAAA-3' (sense) and 5'-AGCTTTTCCAAAAAGGAGGAACTAA CTCTGAAGTCTCTTGAACTTCAGAGTTAGTTCCTCCGGG-3' (antisense) for DDX6i and 5'-GATCCCCGAATCCAGAGGTAATCTACTTCAAGAGA GTAGATTACCTCTGGATTCTTTTTGGAAA-3' (sense) and 5'-AGCTTTTC CAAAAAGAATCCAGAGGTAATCTACTCTCTTGAAGTAGATTACCTC TGGATTCGGG-3' (antisense) for shCon. The oligonucleotides described above were annealed and subcloned into the BglII-HindIII site, downstream from an RNA polymerase III promoter of pSUPER (8), to generate pSUPER-DDX6i and pSUPER-shCon, respectively. To construct pLV-DDX6i and pLV-shCon, the BamHI-SalI fragments of the corresponding pSUPER plasmids were subcloned into the BamHI-SalI site of pRDI292, an HIV-1-derived self-inactivating lentiviral vector containing a puromycin resistance marker allowing for the selection of transduced cells (7). pLV-DDX3i, described previously (3), was used.

Lentiviral vector production. The vesicular stomatitis virus G protein (VSV-G)-pseudotyped HIV-1-based vector system was described previously (27, 44). The lentiviral vector particles were produced by the transient transfection of the second-generation packaging construct pCMV-ΔR8.91 (27, 44), the VSV-G-

envelope-expressing plasmid pMDG2, as well as pRDI292 into 293FT cells with FuGene6 reagent (Roche Diagnostics, Mannheim, Germany).

HCV infection experiments. The supernatants were collected from cell culture-generated HCV-JFH1 (37)-infected RSc cells (3–5, 23) at 5 days postinfection and stored at −80°C after filtering through a 0.45-μm filter (Kurabo, Osaka, Japan) until use. For infection experiments with HCV-JFH1, RSc cells (1 × 10⁵ cells/well) were plated onto 6-well plates and cultured for 24 h. We then infected the cells at a multiplicity of infection (MOI) of 1 or 4. The culture supernatants were collected at 24 h postinfection, and the levels of the core protein were determined by an enzyme-linked immunosorbent assay (ELISA) (Mitsubishi Kagaku Bio-Clinical Laboratories, Tokyo, Japan). Total RNA was also isolated from the infected cellular lysates by using an RNeasy minikit (Qiagen, Hilden, Germany) for analysis of intracellular HCV RNA. The infectivity of HCV-JFH1 in the culture supernatants was determined by a focus-forming assay at 48 h postinfection. HCV-JFH1-infected cells were detected by using anti-HCV core (CP-9 and CP-11 mixture).

Quantitative RT-PCR analysis. The quantitative RT-PCR analysis of HCV RNA was performed by real-time LightCycler PCR (Roche) as described previously (3–5, 14, 23). We used the following forward and reverse primer sets for the real-time LightCycler PCR: 5'-ATGAGTCATGTGGCAGTGGA-3' (forward) and 5'-GCTGGCTGTACTTCCTCCAC-3' (reverse) for DDX3, 5'-ATG AGCACGGCCAGAACAGA-3' (forward) and 5'-TTGCTGTGTCTGTGTGC CCC-3' (reverse) for DDX6, 5'-TGACGGGGTCACCCACACTG-3' (forward) and 5'-AAGCTGTAGCCGCGCTCGGT-3' (reverse) for β-actin, and 5'-AGA GCCATAGTGGTCTGCGG-3' (forward) and 5'-CTTTCGCAACCCAACGC TAC-3' (reverse) for HCV-JFH1.

Preparation of anti-PATL1 antibody. The anti-PATL1 antiserum was raised in rabbits using the glutathione S-transferase (GST)-fused PATL1 Ct (C-terminal region of PATL1, aa 450 to 770) as an antigen, and immunoglobulins were affinity purified by using the maltose-binding protein (MBP)-fused PATL1 Ct that was immobilized on an N-hydroxysuccinimide (NHS) column (GE Healthcare Bio-Sciences AB, Uppsala, Sweden).

Preparation of LDs. Lipid droplets (LDs) were prepared as described previously (26). Cells were pelleted by centrifugation at 1,500 rpm. The pellet was resuspended in hypotonic buffer (50 mM HEPES [pH 7.4], 1 mM EDTA, 2 mM MgCl₂) supplemented with a protease inhibitor cocktail (Nacalai Tesque, Kyoto, Japan) and was incubated for 10 min at 4°C. The suspension was homogenized with 30 strokes of a glass Dounce homogenizer using a tight-fitting pestle (Wheaton, Millville, NJ). A 1/10 volume of 10× isotonic buffer {0.2 M HEPES (pH 7.4), 1.2 M potassium acetate (KoAc), 40 mM magnesium acetate [Mg(oAc)₂], and 50 mM dithiothreitol (DTT)} was added to the homogenate. The nuclei were removed by centrifugation at 2,000 rpm for 10 min at 4°C. The supernatant was collected and centrifuged at 16,000 × g for 10 min at 4°C. The supernatant was mixed with an equal volume of 1.04 M sucrose in isotonic buffer (50 mM HEPES, 100 mM KCl, 2 mM MgCl₂, and protease inhibitor cocktail). The solution was set in a 13.2-ml Polyallomer centrifuge tube (Beckman Coulter, Brea, CA). One milliliter of isotonic buffer was loaded onto the sucrose mixture. The tube was centrifuged at 100,000 × g in an SW41Ti rotor (Beckman Coulter) for 1 h at 4°C. After the centrifugation, the LD fraction on the top of the gradient solution was recovered in phosphate-buffered saline (PBS). The collected LD fraction was used for Western blot analysis.

Western blot analysis. Cells were lysed in a buffer containing 50 mM Tris-HCl (pH 8.0), 150 mM NaCl, 4 mM EDTA, 1% Nonidet P-40, 0.1% sodium dodecyl sulfate (SDS), 1 mM DTT, and 1 mM phenylmethylsulfonyl fluoride. Supernatants from these lysates were subjected to SDS-polyacrylamide gel electrophoresis, followed by immunoblot analysis using anti-DDX3 (catalog no. 54257 [NT] and 5428 [IN]; Anaspec, San Jose, CA), anti-DDX6 (A300-460A; Bethyl Laboratories, Montgomery, TX), anti-adipose differentiation-related protein (ADFP; GTX110204; GeneTex, San Antonio, TX), anti-calnexin (NT; Stressgen, Ann Arbor, MI), anti-HCV core (CP-9 and CP-11; Institute of Immunology, Tokyo, Japan), anti-β-actin antibody (A5441; Sigma, St. Louis, MO), anti-ATX2/SCA2 antibody (A302-033A; Bethyl), anti-PABP (sc-32318 [10E10]; Santa Cruz Biotechnology, Santa Cruz, CA), anti-PABP (ab21060; Abcam, Cambridge, United Kingdom), anti-G3BP1 (611126; BD Transduction Laboratories, San Jose, CA), anti-LSM1 (LS-C97364; Life Span Biosciences, Seattle, WA), anti-HSP70 (610607; BD), anti-XRN1 (A300-443A; Bethyl), or anti-PATL1 antibody.

Immunofluorescence and confocal microscopic analysis. Cells were fixed in 3.6% formaldehyde in PBS, permeabilized in 0.1% NP-40 in PBS at room temperature, and incubated with anti-DDX3 antibody (54257 [NT] and 5428 [IN]; Anaspec), anti-DDX3X (LS-C64576; Life Span), anti-DDX6 (A300-460A; Bethyl), anti-HCV core (CP-9 and CP-11), anti-ATX2/SCA2 antibody (A302-033A; Bethyl), anti-ataxin-2 (611378; BD), anti-PABP (ab21060; Abcam), anti-G3BP1 (A302-033A; Bethyl), anti-LSM1 (LS-C97364; Life Span), anti-XRN1

187

(A300-443A; Bethyl), anti-Dcp2 (A302-597A; Bethyl), anti-human Ago2 (011-22033; Wako, Osaka, Japan), or anti-PATL1 antibody at a 1:300 dilution in PBS containing 3% bovine serum albumin (BSA) for 30 min at 37°C. The cells were then stained with fluorescein isothiocyanate (FITC)-conjugated anti-rabbit antibody (Jackson ImmunoResearch, West Grove, PA) at a 1:300 dilution in PBS containing BSA for 30 min at 37°C. Lipid droplets and nuclei were stained with borondipyrromethene (BODIPY) 493/503 (Molecular Probes, Invitrogen) and DAPI (4′,6-diamidino-2-phenylindole), respectively, for 15 min at room temperature. Following extensive washing in PBS, the cells were mounted onto slides using a mounting medium of 90% glycerin–10% PBS with 0.01% p-phenylenediamine added to reduce fading. Samples were viewed under a confocal laser scanning microscope (LSM510; Zeiss, Jena, Germany).

Statistical analysis. A statistical comparison of the infectivities of HCV in the culture supernatants between the knockdown cells and the control cells was performed by using the Student t test. P values of less than 0.05 were considered statistically significant. All error bars indicate standard deviations.

RESULTS

HCV infection hijacks the P-body components. To investigate the potential role of P-body components in the HCV life cycle, we first examined the alteration of the subcellular localization of DDX3 or DDX6 by HCV-JFH1 infection using confocal laser scanning microscopy as previously described (2), since both DDX3 and DDX6 were identified previously as P-body components (6). For this, we used HuH-7-derived RSc cells, in which cell culture-generated HCV-JFH1 (JFH1 strain of genotype 2a) (37) can infect and effectively replicate (3, 4, 23). HCV-JFH1-infected RSc cells at 60 h postinfection were stained with anti-HCV core antibody, anti-DDX3, and/or anti-DDX6. Lipid droplets (LDs) and nuclei were stained with BODIPY 493/503 and DAPI (4′,6-diamidino-2-phenylindole), respectively. Samples were viewed under a confocal laser scanning microscope. Although we observed that endogenous DDX3 localized in faint cytoplasmic foci in uninfected RSc cells, DDX3 relocalized, formed ringlike structures, and colocalized with the HCV core protein in response to HCV-JFH1 infection (Fig. 1A). On the other hand, endogenous DDX6 was localized in the evident cytoplasmic foci termed P bodies in the uninfected cells (Fig. 1A). DDX6 also relocalized, formed ringlike structures, and colocalized with the core protein in response to HCV-JFH1 infection (Fig. 1A). Although we failed to observe that most of the P bodies of DDX6 perfectly colocalized with DDX3 in uninfected RSc cells (Fig. 1B), we observed a few P bodies of DDX6 colocalized with DDX3 in the uninfected cells (Fig. 1B, arrowheads). Intriguingly, we found that endogenous DDX3 colocalized with endogenous DDX6 in HCV-JFH1-infected cells (Fig. 1B). To further confirm this finding, pHA-DDX3 (41) and pcDNA3-FLAG-DDX6 were cotransfected into 293FT cells. Consequently, we observed that hemagglutinin (HA)-DDX3 colocalized with FLAG-DDX6 in 293FT cells coexpressing HA-DDX3 and FLAG-DDX6 (Fig. 1B), suggesting cross talk of DDX3 with DDX6. Recently, LDs have been found to be involved in an important cytoplasmic organelle for HCV production (26). Indeed, both DDX3 and DDX6 were recruited around LDs in response to HCV infection, while these proteins did not colocalize with LDs in uninfected naïve RSc cells (Fig. 1C). Furthermore, both DDX3 and DDX6 accumulated in the LD fraction of the HCV-JFH1-infected RSc cells; however, we could not detect both proteins in the LD fraction from uninfected control cells (Fig. 1D), suggesting that DDX3 and

DDX6 are recruited around LDs in response to HCV infection.

These results suggest that HCV-JFH1 infection disrupts P-body formation. Therefore, we further examined whether or not HCV-JFH1 disrupts the P-body formations of other microRNA effectors, including Ago2; the Sm-like protein Lsm1, which is a subunit of heptameric-ring Lsm1-7, involved in decapping; the 5′-to-3′ exonuclease Xrn1; the decapping activator PATL1; and the decapping enzyme DCP2 (6, 21, 30). As expected, HCV-JFH1 disrupted the P-body formations of Ago2, Lsm1, and Xrn1 as well as PATL1 (Fig. 2). Lsm1, Xrn1, or PATL1 relocalized, formed ringlike structures, and colocalized with the HCV core protein in response to HCV-JFH1 infection, whereas they were localized predominantly in P bodies in uninfected RSc cells (Fig. 2). In fact, we observed that DDX6 colocalized with Ago2, a P-body marker (Fig. 2). In contrast, HCV-JFH1 failed to disrupt the P-body formation of DCP2 (Fig. 2). Thus, these results suggest that HCV disrupts P-body formation through the hijacking of P-body components.

HCV hijacks stress granule components. Since Nonhoff et al. recently reported that DDX6 interacted with ataxin-2 (ATX2) (28), we examined the potential cross talk among DDX6, ATX2, and HCV. Although ATX2 and G3BP1, a well-known stress granule component (36), were dispersed in the cytoplasm at 37°C, both proteins formed discrete aggregates termed stress granules and colocalized with each other in response to heat shock at 43°C for 45 min, indicating that ATX2 is also stress granule component (Fig. 3A). We did not observe prominent colocalization between DDX6 and ATX2 at 37°C (Fig. 3B). In contrast, we found that DDX6 was recruited, juxtaposed, and partially colocalized with stress granules of ATX2 in response to heat shock at 43°C for 45 min in the uninfected RSc cells (Fig. 3B). Notably, ATX2 was recruited, formed the ring-like structures, and partially colocalized with DDX6 in response to HCV-JFH1 infection even at 37°C (Fig. 3B). Furthermore, we noticed that ATX2 was recruited around LDs in HCV-JFH1-infected cells at 72 h postinfection, while ATX2 did not colocalize with LDs in uninfected cells (Fig. 3C), suggesting the colocalization of ATX2 with the HCV core protein in infected cells. Indeed, ATX2 colocalized with the HCV core protein in HCV-JFH1-infected RSc cells at 37°C (Fig. 3D). Moreover, HCV-JFH1 infection induced the colocalization of the core protein with other stress granule components, G3BP1 or PABP1 as well as ATX2 (Fig. 4 and 5). To further confirm our findings, we examined the time course of the redistribution of DDX6 and G3BP1 after inoculation with HCV-JFH1. Consequently, we still detected the P-body formation of DDX6 and dispersed G3BP1 in the cytoplasm, and we did not observe a colocalization between the HCV core protein and DDX6 at 12 and 24 h postinfection (Fig. 4). In contrast, we found that the P-body formation of DDX6 began to be disrupted at 36 h postinfection (Fig. 4). Consistently, G3BP1 formed stress granules at 36 h postinfection (Fig. 4). We then noticed a ringlike formation of DDX6 or G3BP1 and colocalization with the HCV core protein after 48 h postinfection (Fig. 4), suggesting that the disruption of P-body formation and the hijacking of P-body and stress granule components occur in a late step of HCV infection.
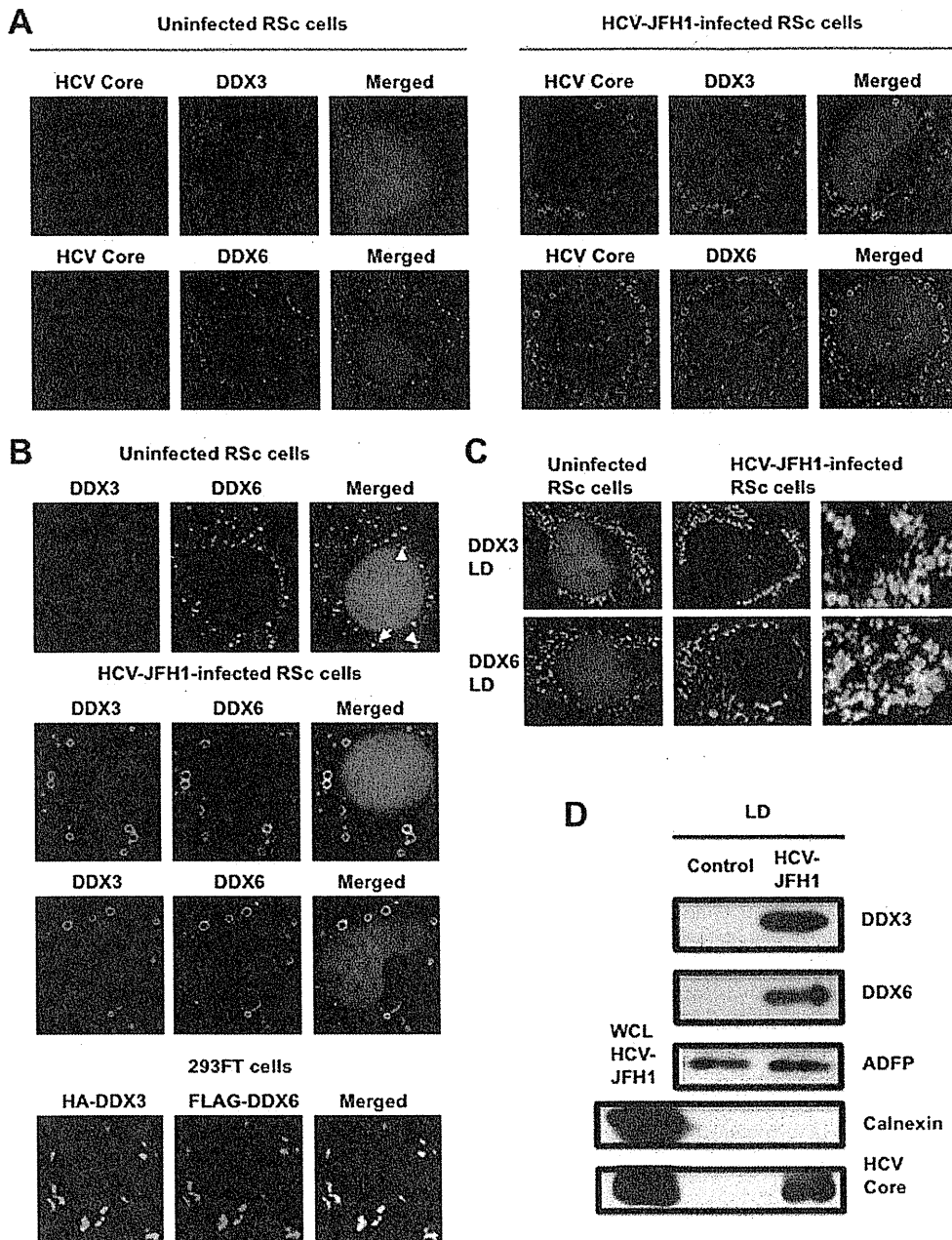
We then examined whether or not HCV-JFH1 infection

FIG. 1. Dynamic recruitment of DDX3 and DDX6 around lipid droplets (LDs) in response to HCV-JFH1 infection. (A) HCV-JFH1 disrupts the P-body formation of DDX6. Cells were fixed at 60 h postinfection and were then examined by confocal laser scanning microscopy. Cells were stained with anti-HCV core (CP-9 and CP-11 mixture) and either anti-DDX3 (54257 and 54258 mixture) or anti-DDX6 (A300-460A) antibody and then visualized with FITC (DDX3 or DDX6) or Cy3 (core). Images were visualized by using confocal laser scanning microscopy. The two-color overlay images are also exhibited (merged). Colocalization is shown in yellow. (B) HCV-JFH1 recruits DDX3 or DDX6 around LDs. Cells were stained with either anti-DDX3 or anti-DDX6 antibody and were then visualized with Cy3 (red). Lipid droplets and nuclei were stained with BODIPY 493/503 (green) and DAPI (blue), respectively. A high-magnification image is also shown. (C) Colocalization of DDX3 with DDX6. HCV-JFH1-infected RSc cells at 60 h postinfection were stained with anti-DDX3X (LS-C64576) and anti-DDX6 (A300-460A) antibodies. 293FT cells cotransfected with 100 ng of pcDNA3-FLAG-DDX6 and 100 ng of pHA-DDX3 (41) were stained with anti-FLAG-Cy3 and anti-HA-FITC antibodies (Sigma). (D) Association of DDX3 and DDX6 with LDs in response to HCV-JFH1 infection. The LD fraction and whole-cell lysates (WCL) were collected from uninfected RSc cells (control) or HCV-JFH1-infected RSc cells at 5 days postinfection. The results of Western blot analyses of DDX3, DDX6, and the HCV core protein as well as the LD marker ADFP and the endoplasmic reticulum (ER) marker calnexin in the LD fraction are shown.
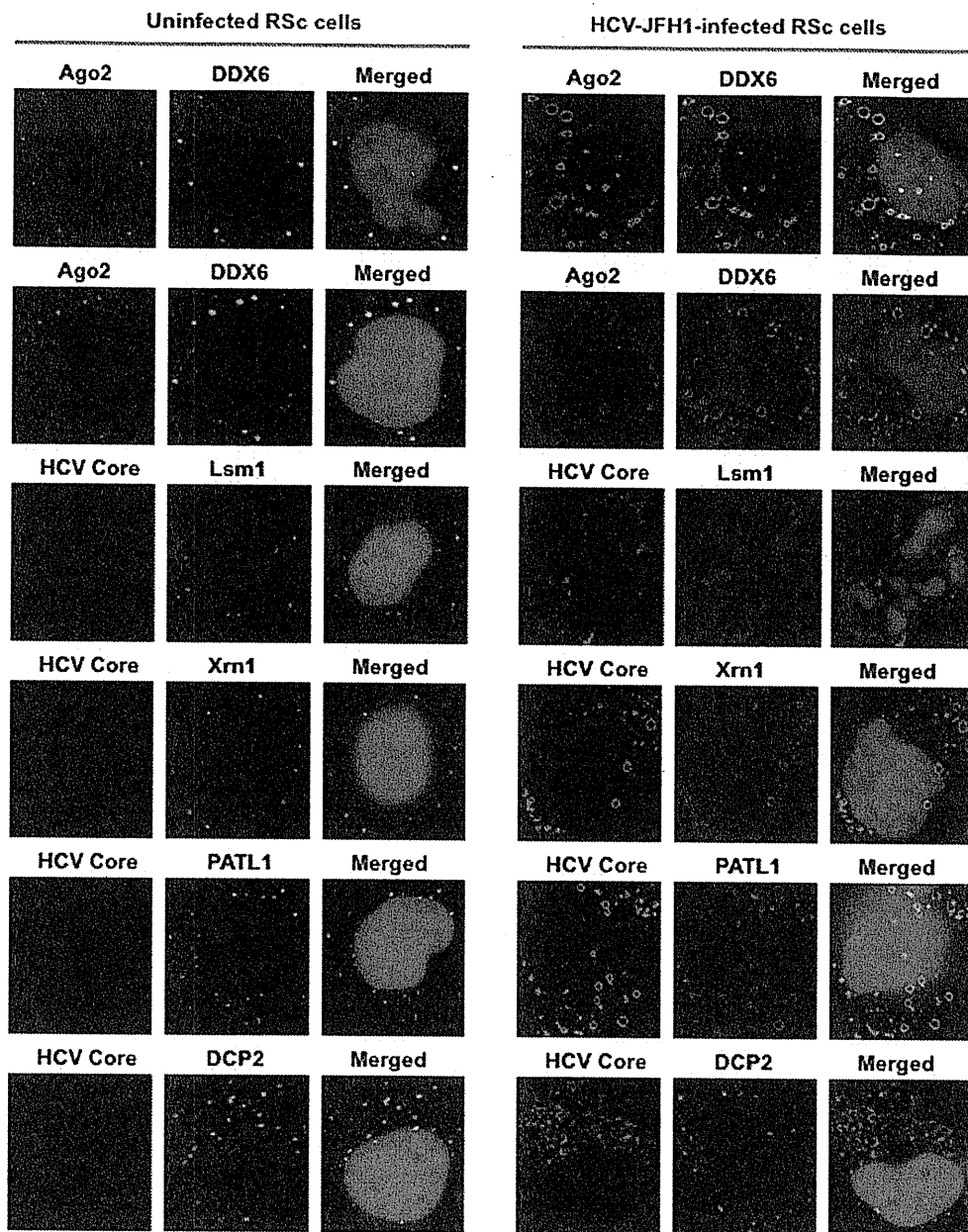
FIG. 2. HCV disrupts the P-body formation of microRNA effectors. Uninfected RSc cells and HCV-JFH1-infected RSc cells at 72 h postinfection were stained with anti-human AGO2 (011-22033) and anti-DDX6 (A300-460A) antibodies. The cells were also stained with anti-HCV core and anti-Lsm1 (LS-C97364), anti-Xrn1 (A300-443A), anti-PATL1, or anti-DCP2 (A302-597A) antibodies and were examined by confocal laser scanning microscopy.

could affect the stress granule formation of G3BP1, ATX2, or PABP1 in response to heat shock or treatment with arsenite. These stress granule components dispersed in the cytoplasm at 37°C, whereas these proteins formed stress granules in response to heat shock at 43°C for 45 min or treatment with 0.5 mM arsenite for 30 min (Fig. 5). In contrast, stress granules were not formed in HCV-JFH1-infected cells at 72 h postinfection in response to heat shock at 43°C for 45 min (Fig. 5), suggesting that HCV-JFH1 infection suppresses stress granule formation in response to heat shock or treatment with arsenite.

Intriguingly, G3BP1, ATX2, or PABP1 still colocalized with the HCV core protein even under the above-described stress conditions (Fig. 5). Furthermore, Western blot analysis of cell lysates of uninfected or HCV-JFH1-infected cells at 72 h postinfection showed similar protein expression levels of ATX2, PABP1, HSP70, DDX3, DDX6, and Lsm1 but not G3BP1 (Fig. 6), suggesting that HCV-JFH1 infection does not affect host mRNA translation.

P-body and stress granule components are required for HCV replication. Finally, we investigated the potential role of
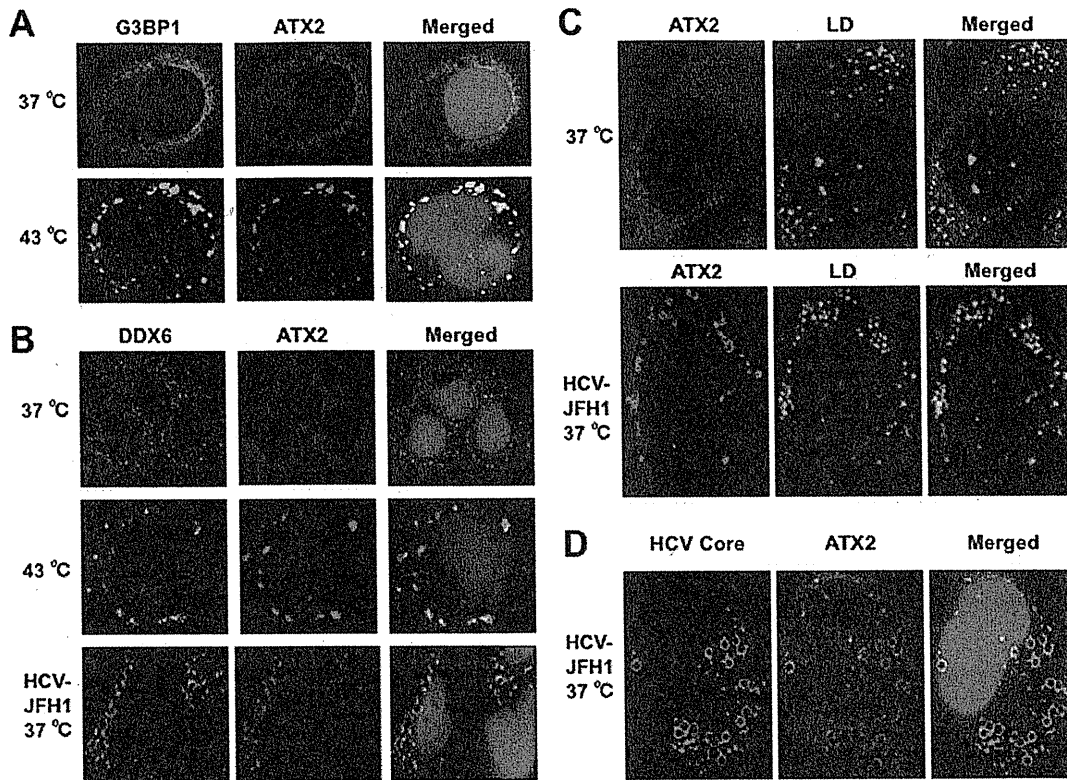
FIG. 3. Dynamic redistribution of ataxin-2 (ATX2) around LDs in response to HCV-JFH1 infection. (A) ATX2 is a stress granule component. RSc cells were incubated at 37°C or 43°C for 45 min. Cells were stained with anti-G3BP1 (A302-033A) and anti-ATX2 (A93520) antibodies and were examined by confocal laser scanning microscopy. (B) Dynamic redistribution of DDX6 and ATX2 in response to heat shock or HCV infection. RSc cells after heat shock at 43°C for 45 min or 72 h after inoculation with HCV-JFH1 were stained with anti-DDX6 and anti-ATX2 (A93520) antibodies. (C) HCV relocalizes ataxin-2 to LDs. HCV-JFH1-infected RSc cells at 72 h postinfection were stained with anti-ATX2 (A93520) antibody and BODIPY 493/503. (D) ATX2 colocalizes with the HCV core protein. HCV-JFH1-infected RSc cells at 72 h postinfection were stained with anti-ATX2/SCA2 (A301-118A) and anti-HCV core antibodies.

P-body and stress granule components in the HCV life cycle. We first used lentiviral vector-mediated RNA interference to stably knock down DDX6 as well as DDX3 in RSc cells. We used puromycin-resistant pooled cells 10 days after lentiviral transduction in all experiments. Real-time LightCycler RT-PCR analysis of DDX3 or DDX6 demonstrated a very effective knockdown of DDX3 or DDX6 in RSc cells transduced with lentiviral vectors expressing the corresponding shRNAs (Fig. 7A). Importantly, shRNAs did not affect cell viabilities (data not shown). We next examined the levels of HCV core and the infectivity of HCV in the culture supernatants as well as the level of intracellular HCV RNA in these knockdown cells 24 h after HCV-JFH1 infection at an MOI of 4. The results showed that the accumulation of HCV RNA was significantly suppressed in DDX3 or DDX6 knockdown cells (Fig. 7B). In this context, the release of the HCV core protein and the infectivity of HCV in the culture supernatants were also significantly suppressed in these knockdown cells (Fig. 7C and D). This finding suggested that DDX6 is required for HCV replication, like DDX3. To further examine the potential role of other P-body and stress granule components in HCV replication, we used RSc cells transiently transfected with a pool of siRNAs specific for ATX2, PABP1, Lsm1, Xrn1, G3BP1, and PATL1 as well as a pool of control siRNAs (siCon) following HCV-

JFH1 infection. In spite of the very effective knockdown of each component (Fig. 7E), the siRNAs used in these experiments did not affect cell viabilities (data not shown). Consequently, the accumulation of HCV RNA was significantly suppressed in ATX2, PABP1, or Lsm1 knockdown cells (Fig. 7F), indicting that ATX2, PABP1, and Lsm1 are required for HCV replication. In contrast, the level of HCV RNA was not affected in Xrn1 knockdown cells (Fig. 7F), suggesting that Xrn1 is unrelated to HCV replication. Furthermore, we observed a moderate effect of siG3BP1 and siPATL1 on HCV RNA replication (Fig. 7F). Altogether, HCV seems to hijack the P-body and stress granule components around LDs for HCV replication.

DISCUSSION

So far, the P body and stress granules have been implicated in mRNA translation, RNA silencing, and RNA degradation as well as viral infection (1, 6, 22, 30). Host factors within the P body and stress granules can enhance or limit viral infection, and some viral RNAs and proteins accumulate in the P body and/or stress granules. Indeed, the microRNA effectors DDX6, GW182, Lsm1, and Xrn1 negatively regulate HIV-1 gene expression by preventing the association of viral mRNA
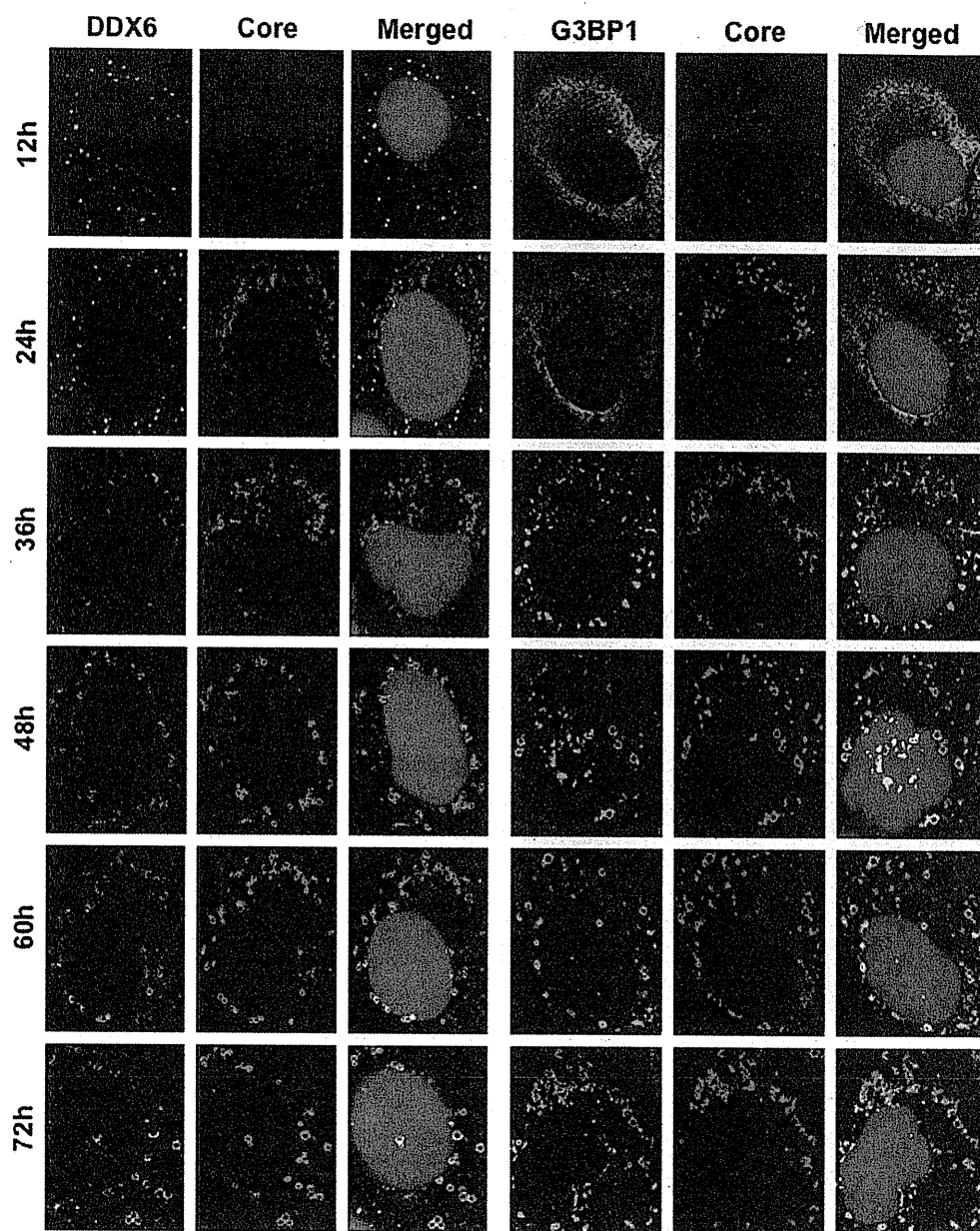
FIG. 4. Dynamic redistribution of DDX6 and G3BP1 in response to HCV-JFH1 infection. RSc cells at the indicated times (hours) after inoculation with HCV-JFH1 were stained with anti-HCV core and either anti-DDX6 (A300-460A) or anti-G3BP1 (A302-033A) antibodies.

with polysomes (9). In contrast, miRNA effectors such as DDX6, Lsm1, PatL1, and Ago2 positively regulate HCV replication (Fig. 7B and F) (16, 31, 33). We have also found that DDX3 and DDX6 are required for HCV RNA replication (3) (Fig. 7B) and that DDX3 colocalized with DDX6 in HCV-JFH1-infected RSc cells (Fig. 1B), suggesting that DDX3 comodulates the DDX6 function in HCV RNA replication. In this regard, the liver-specific miR-122 interacts with the 5'-UTR of the HCV RNA genome and positively regulates HCV replication (15, 17, 19, 20, 31). Since miRNAs usually interact with DDX6 and Ago2 in miRISC and are involved in RNA silencing, DDX6 and Ago2 may be required for miR-122-

dependent HCV replication. Indeed, quite recently, a study showed that Ago2 is required for miR-122-dependent HCV RNA replication and translation (40). However, little is known regarding how miR-122 and DDX6 positively regulate HCV replication. Accordingly, we have shown that these miRNA effectors, including DDX6, Lsm1, Xrn1, and Ago2, accumulated around LDs and the HCV production factory and colocalized with the HCV core protein in response to HCV infection (Fig. 1 and 2). However, the decapping enzyme DCP2 did not accumulate and colocalize with the core protein (Fig. 2). Consistent with this finding, Scheller et al. reported previously that the depletion of DCP2 by siRNA did not affect HCV
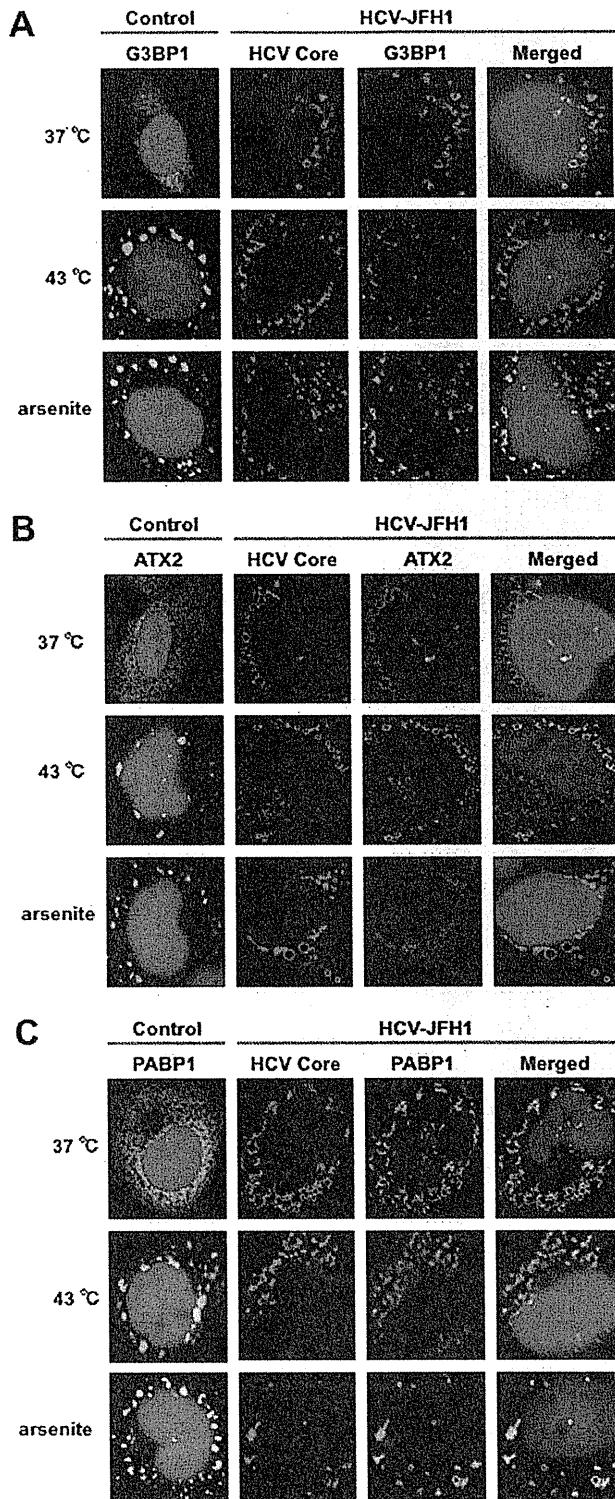
FIG. 5. HCV suppresses stress granule formation in response to heat shock or treatment with arsenite. Naïve RSc cells or HCV-JFH1-infected RSc cells at 72 h postinfection were incubated at 37°C or 43°C for 45 min. Cells were also treated with 0.5 mM arsenite for 30 min. Cells were stained with anti-HCV core and anti-G3BP1 (A), anti-ATX2 (B), or anti-PABP1 (ab21060) (C) antibodies and were examined by confocal laser scanning microscopy.
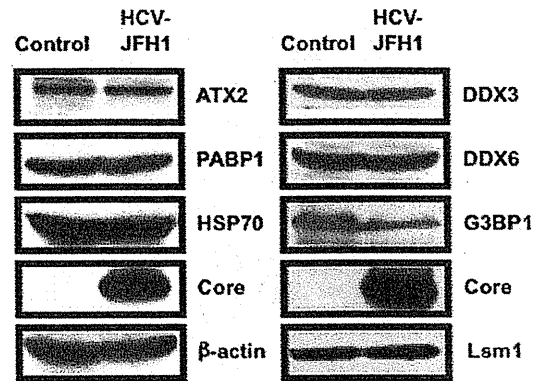

FIG. 6. Host protein expression levels in response to HCV-JFH1 infection. The results of the Western blot analyses of cellular lysates with anti-ATX2/SCA2 antibody (A301-118A), anti-PABP1 (ab21060), anti-HSP70 (610607), anti-HCV core, anti-β-actin, anti-DDX3 (54257 [NT] and 5428 [IN] mixture), anti-DDX6 (A300-460A), anti-G3BP1 (611126), or anti-LSM1 (LS-C97364) antibody in HCV-JFH1-infected RSc cells at 72 h postinfection as well as in naïve RSc cells are shown.

production (33). Since HCV harbors the internal ribosome entry site (IRES) structure in the 5'-UTR of the HCV genome instead of a cap structure, unlike HIV-1, DCP2 may not be recruited on the HCV genome and utilized for HCV replication. Otherwise, DCP2 may determine whether or not DDX6 and miRNAs positively or negatively regulate target mRNA.

Furthermore, we have demonstrated that HCV infection hijacks the P-body and stress granule components around LDs (Fig. 1, 2, 4, and 5). We have found that the P-body formation of DDX6 began to be disrupted at 36 h postinfection (Fig. 4). Consistently, G3BP1 formed stress granules at 36 h postinfection. We then observed the ringlike formation of DDX6 or G3BP1 and colocalization with the HCV core protein after 48 h postinfection, suggesting that the disruption of P-body formation and the hijacking of P-body and stress granule components occur at a late step of HCV infection. Furthermore, HCV infection could suppress stress granule formation in response to heat shock or treatment with arsenite (Fig. 5). In this regard, West Nile virus and dengue virus, of the family *Flaviviridae*, interfere with stress granule formation and P-body assembly through interactions with T cell intracellular antigen 1 (TIA-1)/TIAR (11). Moreover, PABP1 and G3BP1, stress granule components, are known to be common viral targets for the inhibition of host mRNA translation (34, 39). In fact, HIV-1 and poliovirus proteases cleave PABP1 and/or G3BP1 and suppress stress granule formation during viral infection (34, 39). On the other hand, HCV infection transiently induced stress granules at 36 h postinfection (Fig. 4) and did not cleave PABP1 (Fig. 6); however, HCV could suppress stress granule formation in response to heat shock or treatment with arsenite through hijacking their components around LDs, the HCV production factory (Fig. 5). Consistently, Jones et al. showed that HCV transiently induces stress granules of enhanced green fluorescent protein (EGFP)-G3BP at 36 h after infection with the cell culture-generated HCV (HCVcc) reporter virus Jc1FLAG2 (p7-nsGluc2A); however, those authors did not show the recruitment of EGFP-G3BP to LDs (18). Although we do not know the exact reason for this apparent discrepancy,
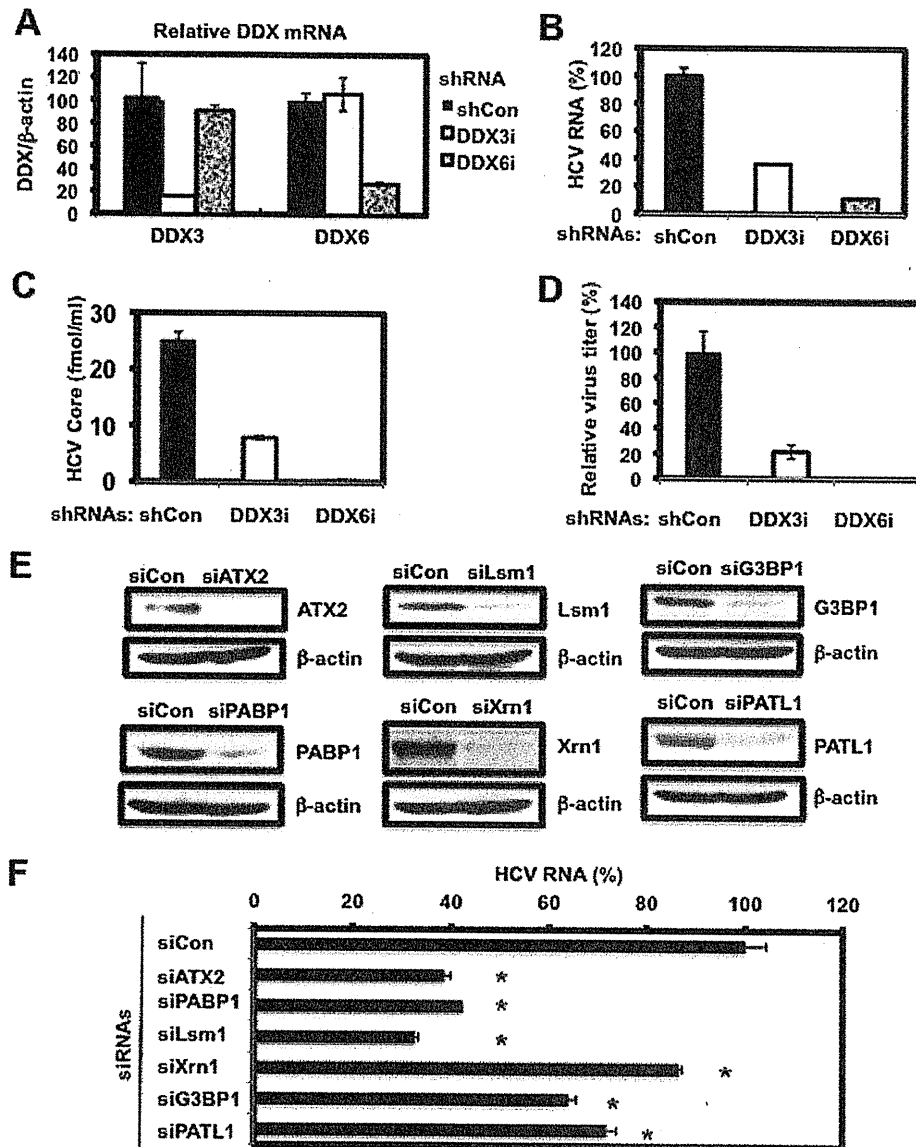
FIG. 7. Requirement of P-body and stress granule components for HCV replication. (A) Inhibition of DDX3 or DDX6 mRNA expression by the shRNA-producing lentiviral vector. Real-time LightCycler RT-PCR for DDX3 or DDX6 was also performed for β-actin mRNA in RSc cells expressing shRNA targeted to DDX3 (DDX3i) or DDX6 (DDX6i) or the control nontargeting shRNA (shCon) in triplicate. Each mRNA level was calculated relative to the level in RSc cells transduced with the control nontargeting lentiviral vector (shCon), which was assigned as 100%. Error bars in this panel and other panels indicate standard deviations. (B) Levels of intracellular genome-length HCV-JFH1 RNA in the cells at 24 h postinfection at an MOI of 4 were monitored by real-time LightCycler RT-PCR. Results from three independent experiments are shown. Each HCV RNA level was calculated relative to the level in RSc cells transduced with a control lentiviral vector (shCon), which was assigned as 100%. (C) The levels of HCV core in the culture supernatants from the stable knockdown RSc cells 24 h after inoculation of HCV-JFH1 at an MOI of 4 were determined by ELISA. Experiments were done in triplicate, and columns represent the mean core protein levels. (D) The infectivity of HCV in the culture supernatants from stable-knockdown RSc cells 24 h after inoculation of HCV-JFH1 at an MOI of 4 was determined by a focus-forming assay at 24 h postinfection. Experiments were done in triplicate, and each virus titer was calculated relative to the level in RSc cells transduced with a control lentiviral vector (shCon), which was assigned as 100%. (E) Inhibition of ATX2, PABP1, Lsm1, Xrn1, G3BP1, or PATL1 protein expression by 72 h after transient transfection of RSc cells with a pool of control nontargeting siRNA (siCon) or a pool of siRNAs specific for ATX2, PABP1, Lsm1, Xrn1, G3BP1, or PATL1 (25 nM), respectively. The results of Western blot analyses of cellular lysates with anti-ATX2, anti-PABP1, anti-Lsm1, anti-Xrn1, anti-G3BP1, anti-PATL1, or anti-β-actin antibody are shown. (F) Levels of intracellular genome-length HCV-JFH1 RNA in the cells at 48 h postinfection at an MOI of 1 were monitored by real-time LightCycler RT-PCR. RSc cells were transiently transfected with a pool of control siRNA (siCon) or a pool of siRNAs specific for ATX2, PABP1, Lsm1, Xrn1, G3BP1, and PATL1 (25 nM). At 48 h after transfection, the cells were inoculated with HCV-JFH1 at an MOI of 1 and incubated for 2 h. The culture medium was then changed and incubated for 22 h. Experiments were done in triplicate, and each HCV RNA level was calculated relative to the level in RSc cells transfected with a control siRNA (siCon), which was assigned as 100%. Asterisks indicate significant differences compared to the control treatment (∗, $P < 0.01$).

several possible explanations can be offered. First, those authors examined the localization of EGFP-G3BP within 48 h postinfection, and we observed it at later times (Fig. 4). Second, they used only EGFP-tagged G3BP instead of endogenous G3BP1. Third, they used a Jc1FLAG2 (p7-nsGluc2A) clone, and an HCV-JFH1 clone could markedly induce the recruitment of the core protein to LDs compared to that of Jc1. Also, Jangra et al. failed to observe the recruitment of DDX6 to LDs at 2 days after infection with HJ3-5 virus (16). Accordingly, we also observed that most of the DDX6 still formed intact P bodies at earlier times (12 h or 24 h postinfection). Importantly, we observed the recruitment of DDX6 to LDs 48 h later (Fig. 4). Furthermore, those authors did not show the ringlike structure formation of the HJ3-5 core protein around LDs, unlike the JFH1 core protein that we used in this study. The interaction of the HCV core protein with DDX6 may explain the recruitment of P-body components to LDs. However, we do not yet know whether the P-body function(s) can be performed on LDs. At least, HCV infection did not affect the translation of several host mRNAs with 5′ caps and 3′ poly(A) tails despite the disruption of P-body formation at 72 h postinfection (Fig. 6), suggesting that HCV does not affect P-body function and that HCV recruits functional P bodies to LDs.

We need to address the potential role of stress granule components, such as PABP1, in HCV replication/translation, since the HCV genome does not harbor the 3′ poly(A) tail. Intriguingly, we have found that the accumulation of HCV RNA was significantly suppressed in PABP1 knockdown RSc cells (Fig. 7F). In this regard, Tingting et al. demonstrated previously that G3BP1 and PABP1 as well as DDX1 were identified as the HCV 3′-UTR RNA-binding proteins by proteomic analysis and that G3BP1 was required for HCV RNA replication (35). Yi et al. also reported that G3BP1 was associated with HCV NS5B and that G3BP1 was required for HCV RNA replication (42). We observed a moderate effect of siG3BP1 on HCV RNA replication (Fig. 7F). In contrast, the accumulation of HCV RNA was significantly suppressed in ATX2 and Lsm1 knockdown cells as well as in PABP1 knockdown cells (Fig. 7F), suggesting that ATX2, Lsm1, and PABP1 are required for HCV replication.

Taking these results together, this study has demonstrated for the first time that HCV hijacks P-body and stress granule components around LDs. This hijacking may regulate HCV RNA replication and translation. Indeed, we have found that the accumulation of genome-length HCV-O (genotype 1b) (14) RNA was markedly suppressed in DDX6 knockdown O cells (data not shown). More importantly, these P-body and stress granule components may be involved in the maintenance of the HCV RNA genome without 5′ cap and 3′ poly(A) tail structures in the cytoplasm for long periods, since the hijacking of P-body and stress granule components by HCV occurred at later times.

ACKNOWLEDGMENTS

REFERENCES

1. Anderson, P., and N. Kedersha. 2007. Stress granules: the Tao of RNA triage. Trends Biochem. Sci. 33:141–150.
2. Ariumi, Y., et al. 2003. Distinct nuclear body components, PML and SMRT, regulate the trans-acting function of HTLV-1 Tax oncoprotein. Oncogene 22:1611–1619.
3. Ariumi, Y., et al. 2007. DDX3 DEAD-box RNA helicase is required for hepatitis C virus RNA replication. J. Virol. 81:13922–13926.
4. Ariumi, Y., et al. 2008. The DNA damage sensors ataxia-telangiectasia mutated kinase and checkpoint kinase 2 are required for hepatitis C virus RNA replication. J. Virol. 82:9639–9646.
5. Ariumi, Y., et al. 2011. The ESCRT system is required for hepatitis C virus production. PLoS One 6:e14517.
6. Beckham, C. J., and R. Parker. 2008. P bodies, stress granules, and viral life cycles. Cell Host Microbe 3:206–212.
7. Bridge, A. J., S. Pebernard, A. Ducraux, A. L. Nicoulaz, and R. Iggo. 2003. Induction of an interferon response by RNAi vectors in mammalian cells. Nat. Genet. 34:263–264.
8. Brummelkamp, T. R., R. Bernard, and R. Agami. 2002. A system for stable expression of short interfering RNAs in mammalian cells. Science 296:550–553.
9. Chable-Bessia, C., et al. 2009. Suppression of HIV-1 replication by microRNA effectors. Retrovirology 6:26.
10. Cristea, I. M., et al. 2010. Host factors associated with the Sindbis virus RNA-dependent RNA polymerase: role for G3BP1 and G3BP2 in virus replication. J. Virol. 84:6720–6732.
11. Emara, M. M., and M. A. Brinton. 2007. Interaction of TIA-1/TIAR with West Nile and dengue virus products in infected cells interferes with stress granule formation and processing body assembly. Proc. Natl. Acad. Sci. U. S. A. 104:9041–9046.
12. Hijikata, M., N. Kato, Y. Ootsuyama, M. Nakagawa, and K. Shimotohno. 1991. Gene mapping of the putative structural region of the hepatitis C virus genome by in vitro processing analysis. Proc. Natl. Acad. Sci. U. S. A. 88:5547–5551.
13. Hijikata, M., et al. 1993. Proteolytic processing and membrane association of putative nonstructural proteins of hepatitis C virus. Proc. Natl. Acad. Sci. U. S. A. 90:10773–10777.
14. Ikeda, M., et al. 2005. Efficient replication of a full-length hepatitis C virus genome, strain O, in cell culture, and development of a luciferase reporter system. Biochem. Biophys. Res. Commun. 329:1350–1359.
15. Jangra, R. K., M. Yi, and S. M. Lemon. 2010. Regulation of hepatitis C virus translation and infectious virus production by the microRNA miR-122. J. Virol. 84:6615–6625.
16. Jangra, R. K., M. Yi, and S. M. Lemon. 2010. DDX6 (Rck/p54) is required for efficient hepatitis C virus replication but not IRES-directed translation. J. Virol. 84:6810–6824.
17. Ji, H., et al. 2008. MicroRNA-122 stimulates translation of hepatitis C virus RNA. EMBO J. 27:3300–3310.
18. Jones, C. T., et al. 2010. Real-time imaging of hepatitis C virus infection using a fluorescent cell-based reporter system. Nat. Biotechnol. 28:167–171.
19. Jopling, C. L., M. Yi, A. M. Lancaster, S. M. Lemon, and P. Sarnow. 2005. Modulation of hepatitis C virus RNA abundance by a liver-specific microRNA. Science 309:1577–1581.
20. Jopling, C. L., S. Schütz, and P. Sarnow. 2008. Position-dependent function for a tandem microRNA miR-122-binding site located in the hepatitis C virus RNA genome. Cell Host Microbe 4:77–85.
21. Kato, N., et al. 1990. Molecular cloning of the human hepatitis C virus genome from Japanese patients with non-A, non-B hepatitis. Proc. Natl. Acad. Sci. U. S. A. 87:9524–9528.
22. Kedersha, N., and P. Anderson. 2007. Mammalian stress granules and processing bodies. Methods Enzymol. 431:61–81.
23. Kuroki, M., et al. 2009. Arsenic trioxide inhibits hepatitis C virus RNA replication through modulation of the glutathione redox system and oxidative stress. J. Virol. 83:2338–2348.
24. Kushima, Y., T. Wakita, and M. Hijikata. 2010. A disulfide-bonded dimer of the core protein of hepatitis C virus is important for virus-like particle production. J. Virol. 84:9118–9127.
25. Mamiya, N., and H. J. Worman. 1999. Hepatitis C virus core protein binds to a DEAD box RNA helicase. J. Biol. Chem. 274:15751–15756.
26. Miyanari, Y., et al. 2007. The lipid droplet is an important organelle for hepatitis C virus production. Nat. Cell Biol. 9:1089–1097.
27. Naldini, L., et al. 1996. In vivo gene delivery and stable transduction of nondividing cells by a lentiviral vector. Science 272:263–267.
28. Nonhoff, U., et al. 2007. Ataxin-2 interacts with the DEAD/H-box RNA helicase DDX6 and interferes with P-bodies and stress granules. Mol. Biol. Cell 18:1385–1396.
29. Owsianka, A. M., and A. H. Patel. 1999. Hepatitis C virus core protein interacts with a human DEAD box protein DDX3. Virology 257:330–340.

30. **Parker, R., and U. Sheth.** 2007. P bodies and the control of mRNA translation and degradation. Mol. Cell **25:**635–646.

31. **Randall, G., et al.** 2007. Cellular cofactors affecting hepatitis C virus infection and replication. Proc. Natl. Acad. Sci. U. S. A. **104:**12884–12889.

32. **Rocak, S., and P. Linder.** 2004. DEAD-box proteins: the driving forces behind RNA metabolism. Nat. Rev. Mol. Cell Biol. **5:**232–241.

33. **Scheller, N., et al.** 2009. Translation and replication of hepatitis C virus genomic RNA depends on ancient cellular proteins that control mRNA fates. Proc. Natl. Acad. Sci. U. S. A. **106:**13517–13522.

34. **Smith, R. W., and N. K. Gray.** 2010. Poly(A)-binding protein (PABP): a common viral target. Biochem. J. **426:**1–11.

35. **Tingting, P., F. Caiyun, Y. Zhigang, Y. Pengyuan, and Y. Zhenghong.** 2006. Subproteomic analysis of the cellular proteins associated with the 3' untranslated region of the hepatitis C virus genome in human liver cells. Biochem. Biophys. Res. Commun. **347:**683–691.

36. **Tourrière, H., et al.** 2003. The RasGAP-associated endoribonuclease G3BP assembles stress granules. J. Cell Biol. **160:**823–831.

37. **Wakita, T., et al.** 2005. Production of infectious hepatitis C virus in tissue culture from a cloned viral genome. Nat. Med. **11:**791–796.

38. **Weston, A., and J. Sommerville.** 2006. Xp54 and related (DDX6-like) RNA helicase: roles in messenger RNP assembly, translation regulation and RNA degradation. Nucleic Acids Res. **34:**3082–3094.

39. **White, J. P., A. M. Cardenas, W. E. Marissen, and R. E. Lloyd.** 2007. Inhibition of cytoplasmic mRNA stress granule formation by a viral proteinase. Cell Host Microbe **2:**295–305.

40. **Wilson, J. A., C. Zhang, A. Huys, and C. D. Richardson.** 2011. Human Ago2 is required for efficient miR-122 regulation of HCV RNA accumulation and translation. J. Virol. **85:**2342–2350.

41. **Yedavalli, V. S., C. Neuveut, Y. H. Chi, L. Kleiman, and K. T. Jeang.** 2004. Requirement of DDX3 DAED box RNA helicase for HIV-1 Rev-RRE export function. Cell **119:**381–392.

42. **Yi, Z., et al.** 2006. Subproteomic study of hepatitis C virus replicon reveals Ras-GTPase-activating protein binding protein 1 as potential HCV RC component. Biophys. Biochem. Res. Commun. **350:**174–178.

43. **You, L. R., et al.** 1999. Hepatitis C virus core protein interacts with cellular putative RNA helicase. J. Virol. **73:**2841–2853.

44. **Zufferey, R., D. Nagy, R. J. Mandel, L. Naldini, and D. Trono.** 1997. Multiply attenuated lentiviral vector achieves efficient gene delivery in vivo. Nat. Biotechnol. **15:**871–875.

196

PLoS one

The ESCRT System Is Required for Hepatitis C Virus Production

Yasuo Ariumi[1]*, Misao Kuroki[1], Masatoshi Maki[2], Masanori Ikeda[1], Hiromichi Dansako[1], Takaji Wakita[3], Nobuyuki Kato[1]

1 Department of Tumor Virology, Okayama University Graduate School of Medicine, Dentistry, and Pharmaceutical Sciences, Okayama, Japan, 2 Department of Applied Molecular Biosciences, Graduate School of Bioagricultural Sciences, Nagoya University, Nagoya, Japan, 3 Department of Virology II, National Institute of Infectious Diseases, Tokyo, Japan

Abstract

Background: Recently, lipid droplets have been found to be involved in an important cytoplasmic organelle for hepatitis C virus (HCV) production. However, the mechanisms of HCV assembly, budding, and release remain poorly understood. Retroviruses and some other enveloped viruses require an endosomal sorting complex required for transport (ESCRT) components and their associated proteins for their budding process.

Methodology/Principal Findings: To determine whether or not the ESCRT system is needed for HCV production, we examined the infectivity of HCV or the Core levels in culture supernatants as well as HCV RNA levels in HuH-7-derived RSc cells, in which HCV-JFH1 can infect and efficiently replicate, expressing short hairpin RNA or siRNA targeted to tumor susceptibility gene 101 (TSG101), apoptosis-linked gene 2 interacting protein X (Alix), Vps4B, charged multivesicular body protein 4b (CHMP4b), or Brox, all of which are components of the ESCRT system. We found that the infectivity of HCV in the supernatants was significantly suppressed in these knockdown cells. Consequently, the release of the HCV Core into the culture supernatants was significantly suppressed in these knockdown cells after HCV-JFH1 infection, while the intracellular infectivity and the RNA replication of HCV-JFH1 were not significantly affected. Furthermore, the HCV Core mostly colocalized with CHMP4b, a component of ESCRT-III. In this context, HCV Core could bind to CHMP4b. Nevertheless, we failed to find the conserved viral late domain motif, which is required for interaction with the ESCRT component, in the HCV-JFH1 Core, suggesting that HCV Core has a novel motif required for HCV production.

Conclusions/Significance: These results suggest that the ESCRT system is required for infectious HCV production.

Introduction

Hepatitis C virus (HCV) is a causative agent of chronic hepatitis, which progresses to liver cirrhosis and hepatocellular carcinoma. HCV is an enveloped virus with a positive single stranded 9.6 kb RNA genome, which encodes a large polyprotein precursor of approximately 3,000 amino acid residues. This polyprotein is cleaved by a combination of the host and viral proteases into at least 10 proteins in the following order: Core, envelope 1 (E1), E2, p7, nonstructural protein 2 (NS2), NS3, NS4A, NS4B, NS5A, and NS5B [1]. HCV Core, a highly basic RNA-binding protein, forms a viral capsid and is targeted to lipid droplets [2–6]. The Core is essential for infectious virion production [7]. NS5A, a membrane-associated RNA-binding phosphoprotein, is also involved in the assembly and maturation of infectious HCV particles [8,9]. Intriguingly, NS5A is a key regulator of virion production through the phosphorylation by casein kinase II [9]. Recently, lipid droplets have been found to be

involved in an important cytoplasmic organelle for HCV production [4]. Indeed, NS5A is known to colocalize with the Core on lipid droplets [5], and the interaction between NS5A and the Core is critical for the production of infectious HCV particles [3]. However, the host factor involved in HCV assembly, budding, and release remains poorly understood.

Budding is an essential step in the life cycle of enveloped viruses. Endosomal sorting complex required for transport (ESCRT) components and associated factors, such as tumor susceptibility gene 101 (TSG101, a component of ESCRT-I), charged multivesicular body protein 4b (CHMP4b, a component of ESCRT-III), and apoptosis-linked gene 2 interacting protein X (ALIX, a TSG101- and CHMP4b-binding protein), have been found to be involved in membrane remodeling events that accompany endosomal protein sorting, cytokinesis, and the budding of several enveloped viruses, such as human immunodeficiency virus type 1 (HIV-1) [10–12]. The ESCRT complexes I, II, and III are sequentially, or perhaps concentrically recruited to the endosomal membrane to sequester

cargo proteins and drive vesicularization into the endosome. Finally, ESCRT-III recruits Vps4 (two isoforms, Vps4A and Vps4B), a member of the AAA-family of ATPase that disassembles and thereby terminates and recycles the ESCRT machinery.

Since HCV is also an enveloped RNA virus, we hypothesized that the ESCRT system might be required for HCV production. To test this hypothesis, we examined the release of HCV Core into culture supernatants from cells rendered defective for ESCRT components by RNA interference. The results provide evidence that the ESCRT system is required for HCV production.

Materials and Methods

Cell Culture

293FT cells (Invitrogen, Carlsbad, CA) were cultured in Dulbecco's modified Eagle's medium (DMEM; Invitrogen) supplemented with 10% fetal bovine serum (FBS). The HuH-7-derived cell line, RSc cured cells that cell culture-generated HCV-JFH1 (JFH1 strain of genotype 2a) [13] could infect and effectively replicate [14–16] and OR6c and OR6 cells harboring the genome-length HCV-O RNA with luciferase as a reporter were cultured in DMEM with 10% FBS as described previously [17,18].

Plasmid Construction

To construct pcDNA3-FLAG-Alix, a DNA fragment encoding Alix was amplified from total RNAs derived from RSc cells by RT-PCR using the follwing pairs of primers: Forward 5′-CGGG-ATCCAAGATGGCGACATTCATCTCGGT-3′ and reverse 5′-CCGGCGGCCGCTTACTGCTGTGGATAGTAAG-3′. The obtained DNA fragment was subcloned into BamHI-NotI of pcDNA3-FLAG vector [19], and the nucleotide sequences were determined by Big Dye termination cycle sequencing using an ABI Prism 310 genetic analyzer (Applied Biosystems, Foster City, CA, USA). The plasmid of pJRN/3-5B was based on pJFH1 [13] and was constructed as previously described [20].

RNA synthesis, RNA transfection, and Selection of G418-resistant cells

Plasmid pJRN/3-5B were linearized by XbaI and used for the RNA synthesis with the T7 MEGAScript kit (Ambion, Austin, TX). In vitro transcribed RNA was transfected into OR6c cells by electroporation [17,18]. The transfected cells were selected in culture medium containing G418 (0.3 mg/ml) for 3 weeks. We referred to them as OR6c/JRN 3-5B cells.

Immunofluorescence and Confocal Microscopic Analysis

Cells were fixed in 3.6% formaldehyde in phosphate-buffered saline (PBS) and permeabilized in 0.1% Nonidet P-40 (NP-40) in PBS at room temperature as previously described [21]. Cells were incubated with anti-HCV Core antibody (CP-9 and CP-11 mixture; Institute of Immunology, Tokyo, Japan), anti-Myc-Tag antibody (PL14; Medical & Biological Laboratories, MBL, Nagoya, Japan), anti-Alix antibody (Covalab, Villeurbanne, France), and/or anti-FLAG polyclonal antibody (Sigma, St. Louis, MO) at a 1:300 dilution in PBS containing 3% bovine serum albumin (BSA) at 37°C for 30 min. Cells were then stained with fluorescein isothiocyanate (FITC)-conjugated anti-rabbit antibody (Jackson ImmunoResearch, West Grove, PA) or anti-Cy3-conjugated anti-mouse antibody (Jackson ImmunoResearch) at a 1:300 dilution in PBS containing BSA at 37°C for 30 min. Lipid droplets and nuclei were stained with BODIPY 493/503 (Molecular Probes, Invitrogen) and DAPI (4′,6′-diamidino-2-phenylindole), respectively. Following extensive washing in PBS, cells were mounted on slides using a mounting media of 90%

glycerin/10% PBS with 0.01% p-phenylenediamine added to reduce fading. Samples were viewed under a confocal laser-scanning microscope (LSM510; Zeiss, Jena, Germany).

RNA Interference

The following siRNAs were used: human TSG101 (siGEN-OME SMARTpool M-003549-01-0005 and 5′-CCUCCAGU-CUUCUCUCGUCUU-3′ sense, 5′-GACGAGAGAAGACUG-GAGGUU-3′ antisense), human Alix/PDCD6IP (siGENOME SMARTpool M-004233-02-0005), human Vps4B (siGENOME SMARTpool M-013119-02-0005), human CHMP4b (siGEN-OME SMARTpool M-018075-00-0005), and siGENOME Non-Targeting siRNA Pool#1 (D-001206-13-05) (Dharmacon, Thermo Fisher Scientific, Waltham, MA) as a control. siRNAs (50 nM final concentration) were transiently transfected into either RSc cells [14–16] or OR6 cells [17,18] using Oligofectamine (Invitrogen) according to the manufacturer's instructions. Oligo-nucleotides with the following sense and antisense sequences were used for the cloning of short hairpin (sh) RNA-encoding sequences against TSG101, Alix, Vps4B, or CHMP4b in lentiviral vector: TSG101i, 5′-GATCCCC GGAGGAAATGGATCGTGCCTT-CAAGAGAGGCACGATCCATTTCCTCCTTTTTGGAAA-3′ (sense), 5′-AGCTTTTCCAAAAAGGAGGAAATGGATCGTG-CCTCTCTTGAAGGCACGATCCATTTCCTCCGGG-3′ (an-tisense); Alixi, 5′-GATCCCC GGAGGTGTTCCCTGTCTTG-TTCAAGAGACAAGACAGGGAACACCTCCTTTTTGGAA-A-3′ (sense), 5′-AGCTTTTCCAAAAAGGAGGTGTTCCCTG-TCTTGTCTCTTGAACAAGACAGGGAACACCTCCGGG-3′ (antisense); Vps4Bi, 5′-GATCCCC GGAGAATCTGATGATC-CTGTTCAAGAGACAGGATCATCAGATTCTCCTTTTTG-GAAA-3′ (sense), 5′-AGCTTTTCCAAAAAGGAGAATCT-GATGATCCTGTCTCTTGAACAGGATCATCAGATTCTC-CGGG-3′ (antisense); CHMP4bi, 5′-GATCCCC GAGGAG-GACGACGACATGATTCAAGAGATCATGTCGTCGTCC-TCCTCTTTTTGGAAA-3′ (sense), 5′-AGCTTTTCCAAAAA-GAGGAGGACGACGACATGATCTCTTGAATCATGTCG-TCGTCCTCCTCGGG-3′ (antisense); Broxi, 5′-GATCCCCG-GATGACAGTACTAAACCCTTCAAGAGAGGGTTTAGTA-CTGTCATCCTTTTTGGAAA-3′ (sense), 5′-AGCTTTTC-CAAAAAGGATGACAGTACTAAACCCTCTCTTGAAGGG-TTTAGTACTGTCATCCGGG-3′ (antisense). The oligonucleo-tides above were annealed and subcloned into the BglII-HindIII site, downstream from an RNA polymerase III promoter of pSUPER [22], to generate pSUPER-TSG101i, pSUPER-Alixi, pSUPER-Vps4Bi, and pSUPER-CHMP4bi, respectively. To construct pLV-TSG101i, pLV-Alixi, pLV-Vps4Bi, and pLV-CHMP4bi, the BamHI-SalI fragments of the corresponding pSUPER plasmids were subcloned into the BamHI-SalI site of pRDI292 [23], an HIV-1-derived self-inactivating lentiviral vector containing a puromycin resistant marker allowing for the selection of transduced cells, respectively.

Lentiviral Vector Production

The vesicular stomatitis virus (VSV)-G-pseudotyped HIV-1-based vector system has been described previously [24–26]. The lentiviral vector particles were produced by transient transfection of the second-generation packaging construct pCMV-ΔR8.91 [24–26] and the VSV-G-envelope-expressing plasmid pMDG2 as well as pRDI292 into 293FT cells with FuGene6 (Roche Diagnostics, Basel, Switzerland).

HCV Infection Experiments

The supernatants was collected from cell culture-generated HCV-JFH1 [13]-infected RSc cells [14–16] at 5 days post-

198